JACS
JOURNAL OF THE AMERICAN CHEMICAL SOCIETY

Subscriber access provided by UNIV OF DURHAM

Bimolecular Coupling as a Vector for Decomposition of Fast-Initiating Olefin Metathesis Catalysts

Gwendolyn A Bailey, Marco Foscato, Carolyn S. Higman, Craig S. Day, Vidar R. Jensen, and Deryn Elizabeth Fogg

J. Am. Chem. Soc., **Just Accepted Manuscript** • DOI: 10.1021/jacs.8b02709 • Publication Date (Web): 13 Apr 2018

Downloaded from http://pubs.acs.org on April 13, 2018

Just Accepted

"Just Accepted" manuscripts have been peer-reviewed and accepted for publication. They are posted online prior to technical editing, formatting for publication and author proofing. The American Chemical Society provides "Just Accepted" as a service to the research community to expedite the dissemination of scientific material as soon as possible after acceptance. "Just Accepted" manuscripts appear in full in PDF format accompanied by an HTML abstract. "Just Accepted" manuscripts have been fully peer reviewed, but should not be considered the official version of record. They are citable by the Digital Object Identifier (DOI®). "Just Accepted" is an optional service offered to authors. Therefore, the "Just Accepted" Web site may not include all articles that will be published in the journal. After a manuscript is technically edited and formatted, it will be removed from the "Just Accepted" Web site and published as an ASAP article. Note that technical editing may introduce minor changes to the manuscript text and/or graphics which could affect content, and all legal disclaimers and ethical guidelines that apply to the journal pertain. ACS cannot be held responsible for errors or consequences arising from the use of information contained in these "Just Accepted" manuscripts.

ACS Publications

is published by the American Chemical Society. 1155 Sixteenth Street N.W., Washington, DC 20036

Published by American Chemical Society. Copyright © American Chemical Society. However, no copyright claim is made to original U.S. Government works, or works produced by employees of any Commonwealth realm Crown government in the course of their duties.

Bimolecular Coupling as a Vector for Decomposition of Fast-Initiating Olefin Metathesis Catalysts

Gwendolyn A. Bailey,[†] Marco Foscato,[‡] Carolyn S. Higman,[†] Craig S. Day,[†] Vidar R. Jensen,[‡] Deryn E. Fogg*,[†]

[†]Center for Catalysis Research and Innovation, and Department of Chemistry and Biomolecular Sciences, University of Ottawa, Ottawa, ON, Canada K1N 6N5. [‡]Department of Chemistry, University of Bergen, Allégaten 41, N-5007 Bergen, Norway

KEYWORDS: Olefin metathesis, catalyst decomposition, bimolecular coupling, catalyst initiation, high activity

ABSTRACT: The correlation between rapid initiation and rapid decomposition in olefin metathesis is probed for a series of fast-initiating Ru catalysts: the Hoveyda catalyst **HII**, $RuCl_2(L)(=CHC_6H_4$-*o*-$O^iPr)$; the Grela catalyst **nG** (a derivative of **HII** with a nitro group *para* to O^iPr); the Piers catalyst **PII**, $[RuCl_2(L)(=CHPCy_3)]OTf$; the third-generation Grubbs catalyst **GIII**, $RuCl_2(L)(py)_2(=CHPh)$; and dianiline catalyst **DA**, $RuCl_2(L)$(*o*-dianiline)(=CHPh) (L = H_2IMes = *N,N'*-bis (mesityl)-imidazolin-2-ylidene). Prior studies of ethylene metathesis established that various Ru metathesis catalysts can decompose by β-elimination of propene from metallacyclobutane $RuCl_2(H_2IMes)(\kappa^2$-$C_3H_6)$ **Ru-2**. The present work demonstrates that in metathesis of terminal olefins, β-elimination yields only ca. 25–40% propenes for **HII**, **nG**, **PII** or **DA**, and *none* for **GIII**. The discrepancy is attributed to competing decomposition via bimolecular coupling of methylidene intermediate $RuCl_2(H_2IMes)(=CH_2)$ **Ru-1**. Direct evidence for methylidene coupling is presented, via the controlled decomposition of transiently-stabilized adducts of **Ru-1**, $RuCl_2(H_2IMes)L_n(=CH_2)$ (L_n = $py_{n'}$; n' = 1, 2, or *o*-dianiline). These adducts were synthesized by treating in situ-generated metallacyclobutane **Ru-2** with pyridine or *o*-dianiline, and isolated at low temperature (–116 °C or –78 °C, respectively). On warming, both undergo methylidene coupling, liberating ethylene and forming $RuCl_2(H_2IMes)L_n$. A mechanism is proposed based on kinetic studies and molecular-level computational analysis. Bimolecular coupling emerges as an important contributor to the instability of **Ru-1**, and a potentially major pathway for decomposition of fast-initiating, phosphine-free metathesis catalysts.

INTRODUCTION

Olefin metathesis represents an exceptionally powerful, general methodology for the catalytic assembly of carbon-carbon bonds.[1] Ru-catalyzed olefin metathesis, long embraced in academia, is now beginning to see industrial uptake.[2] Reports from pharmaceutical manufacturing, however, highlight catalyst productivity as a challenge in process chemistry.[2] Improved understanding of catalyst decomposition, particularly the pathways operative for the most vulnerable active species (Chart 1), is critical to guide process implementation and catalyst redesign.

Chart 1. Key Active Species in Olefin Metathesis.

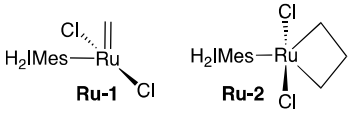

The ease with which catalysts enter and exit the active cycle is fundamental to their productivity and stability. To aid in systematic analysis, the classification scheme in Chart 2 is proposed. Class A metathesis catalysts, exemplified by the second-generation Grubbs catalyst **GII**, initiate slowly, but the ligand dissociated from the precatalyst is slow to recapture the active species **Ru-1**.[3] Class B catalysts (e.g. **HII** or the recently-reported[4] dianiline catalyst **DA**) initiate readily, but recapture of the active species is facile, resulting in rapid shuttling into and out of the catalytic cycle.[3,5] Class C catalysts (e.g. the third-generation Grubbs catalyst **GIII**, the Grela catalyst **nG**, or the Piers catalyst **PII**) also initiate rapidly, and recapture of **Ru-1** by the released ligand is minimal.[3,6] The trade-off between activity and stability evident from recent prominent reviews[7] underscores the importance of understanding the decomposition pathways for fast-initiating Class B/C metathesis catalysts, in particular.

Chart 2. Classification of Metathesis Catalysts.

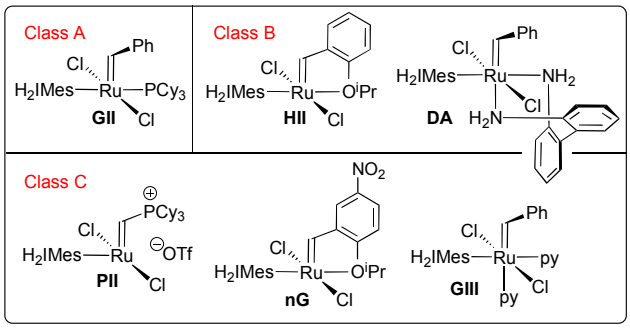

Intrinsic Decomposition Pathways Established for the Dominant Ru Metathesis Catalysts. The decomposition chemistry intrinsic to the PCy_3-stabilized catalysts of Class A has been extensively studied. **GII**, for example, although robust as the precatalyst, readily decomposes once converted into the metathesis-active methylidene intermediate **Ru-1**. Methylidene abstraction from **Ru-1** by free PCy_3 (Scheme 1a) is widely documented,[8,9] although nucleophilic primary amines such as $NH_2{}^nBu$ can compete to abstract this key ligand.[9d] For phosphine-free Class B/C catalysts such as **HII** and **PII**, the sole *intrinsic* decomposition pathway for which experimental evidence has been reported to date is depicted in Scheme 1b. β-Hydride elimination from the metallacyclobutane intermediate **Ru-2** generates an allyl hydride, from which propene is liberated by reductive elimination. Evidence for this pathway was established by the Piers group, via synthesis of an isotopologue of **Ru-2** bearing a ^{13}C-labelled metallacyclobutane ring. Decomposition of the labelled complex afforded $^{13}C_3H_6$, unequivocally confirming the origin of the propene byproduct in the metallacyclobutane ring.[10] Of note, Eisenstein and coworkers reported that β-H transfer within the metallacyclobutane intermediate is also the key initial step in decomposition of d^0 ML_4 olefin metathesis catalysts.[11]

Scheme 1. Intrinsic Decomposition Pathways for Catalysts of Classes A–C (where L = H_2IMes).[a]

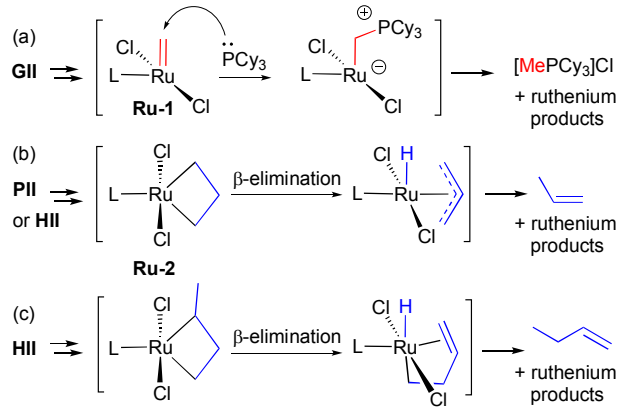

[a]The proton required to eliminate the σ-alkyl ligand in path (a) is supplied by cyclometallation of the H_2IMes ligand.[9a]

Bespalova and co-workers likewise invoked β-elimination / reductive elimination from **Ru-2** to account for formation of propene upon heating **HII** in the presence of ethylene.[12,13] Propene is thus a key marker for the β-elimination pathway in these experiments. (Caution must be exercised, however, to ensure that no Brønsted base is present that can generate propenes via an alternative process, which commences with metallacyclobutane deprotonation).[14,15]

A related pathway was proposed based on density functional theory (DFT) calculations, for terminal olefins bearing a suitable aliphatic substituent.[16] For substrates in which an exocyclic β-H is present, expansion of the metallacyclobutane ring was predicted, with ultimate loss of this ligand as an olefin (Scheme 1c).

In comparison, the decomposition of pyridine-stabilized catalysts such as **GIII** is poorly understood. Sponsler and coworkers reported that **GIII^{Br}** (in which the pyridine ligands are 3-bromopyridine) decomposed within seconds on exposure to ethylene.[17] Hong and Grubbs[8a] undertook the corresponding reaction of **GIII** with ethylene, with the intention of synthesizing methylidene species **GIIIm** (Scheme 2). The latter complex, a pyridine analogue of **GIIm** $RuCl_2(H_2IMes)(PCy_3)(=CH_2)$ (the resting state species formed in metathesis by **GII**), was too unstable even to observe in situ at RT. Instead, the sole product identified was the tris-pyridine derivative **Ru-3**. (**Ru-3** was also formed, and crystallographically characterized, on decomposition of **GIIm** in the presence of pyridine).[8a] The absence of [Me-py]Cl in these reactions was explicitly noted, indicating that pyridine – unlike PCy_3 or primary amines – is insufficiently nucleophilic[18] (or insufficiently basic) to attack the methylidene ligand. The fate of the methylidene ligand was not determined.

Scheme 2. Reported Decomposition Behavior of GIII.[a]

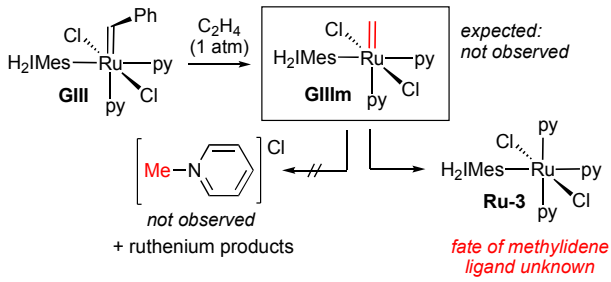

[a]Loss of [Me-py]$^+$ via deprotonation (cyclometallation) of H_2IMes was postulated: cf. footnote a in Scheme 1a.

Proposed Role for Bimolecular Coupling. We speculated that bimolecular coupling of the 14-electron intermediate **Ru-1**, with elimination of the methylidene ligands as ethylene, might contribute to decomposition for *all* of the fast-initiating Ru metathesis catalysts. This pathway would go unrecognized during the "ethenolysis" experiments described above, because ethylene (the marker for methylidene coupling) is masked by the reagent gas.

By the same token, any methylidene coupling during metathesis of 1-olefins – the majority of substrates – would be masked by ethylene formed as the coproduct of metathesis.

Bimolecular coupling has been extensively documented for d^0 metathesis catalysts, and is indeed well established across group 3-7 chemistry.[7,19] The rate of decomposition is, unsurprisingly, sensitive to the bulk of R in the [M]=CHR species: accordingly, it is generally rapid for methylidene species, and much slower for complexes containing bulky alkylidenes. In some cases, the ethylene liberated by coupling of methylidene complexes afforded isolable ethylene adducts, an important aid in confirming the operation of bimolecular coupling.[7,19] Although bimolecular coupling is also widely accepted for "first-generation" Ru catalysts,[7] it is regarded as considerably less likely for the important Ru-NHC catalysts, owing in part to the steric impediment to approach of two $RuCl_2(NHC)(=CH_2)$ molecules.[20] It is undoubtedly inhibited for **GII** and its resting-state species **GIIm**, for which slow loss of PCy_3 limits the concentration of **Ru-1** present at any given time. Rapid olefin binding to **Ru-1** (a distinct feature of the NHC catalysts, which led Chen to term them "high commitment",[21] and Piers "olefinophilic"[10b]) further limits the concentration of **Ru-1**. Finally, the kinetically dominant decomposition pathway for **GII** during metathesis is typically abstraction of the methylidene ligand by free PCy_3, as shown in Scheme 1a above.[8,9]

For phosphine-free **HII**, bimolecular coupling is thought to be limited by facile "boomerang" recapture of **Ru-1** by free isopropoxystyrene.[5] This proposition is difficult to examine, however. **HII** itself is sterically protected against such coupling, while the active methylidene intermediate **Ru-1** is spectroscopically unobservable. Important alternative opportunities for insight are offered by the *o*-dianiline catalyst **DA** and pyridine catalyst **GIII**. We considered that the labile *N*-donor ligands in these precatalysts could offer potential access to transiently-stabilized methylidene species (that is, adducts of **Ru-1**), if suitable synthetic routes could be envisaged. Here we report the successful low-temperature synthesis of such adducts, and the first direct evidence that bimolecular coupling, with loss of the methylidene ligand as ethylene, represents a major pathway for decomposition of Class B/C metathesis catalysts. Further, we demonstrate that the contribution of this pathway to decomposition of **HII**, the dominant Class B catalyst in current use, has almost undoubtedly been underestimated.

RESULTS AND DISCUSSION

Quantifying Decomposition via β-Elimination. Prior studies of the decomposition of phosphine-free ruthenium metathesis catalysts, as noted above, focused on the behavior of **PII** and **HII** under ethylene. The observation of propene in these experiments provided important qualitative evidence for β-elimination from the metallacyclobutane **Ru-2** (Scheme 1b). However, the yield of propene based on Ru, and hence the extent of this pathway, was not determined.

We therefore began by seeking to quantify the propene byproducts generated during styrene metathesis. Here propene and β-methylstyrene (Figure 1) serve as markers for catalyst decomposition via β-elimination from **Ru-2** or a Ph-substituted metallacyclobutane, respectively. This experiment serves two purposes. First, it reports on the importance of this decomposition route. Secondly, it shifts the focus to 1-olefins, a family of metathesis substrates of very broad relevance. Styrene is chosen because, unlike most 1-olefins, it cannot isomerize. This is critical to prevent formation of "false" propenyl markers: that is, propenes formed by isomerization-metathesis (see SI, Section S1), rather than β-elimination.

Accordingly, metathesis of styrene was undertaken with **HII**, **nG**, **GIII**, **PII**, and **DA** (1 mol%; Figure 1). These experiments were carried out in NMR tubes completely filled with solvent,[22] to minimize loss of volatile propene to the headspace. This results in co-retention of ethylene, which was expected to maximize formation of metallacyclobutane **Ru-2**, and consequently propene elimination. Notably, however, *no* propenes were observed for **GIII**, and <40% propenes for **HII**, **nG**, **PII**, and **DA**. Clearly, some additional decomposition pathway is operative. If bimolecular coupling indeed accounts for the balance, it is a much more significant contributor to decomposition of Class B/C catalysts than has been considered to date.

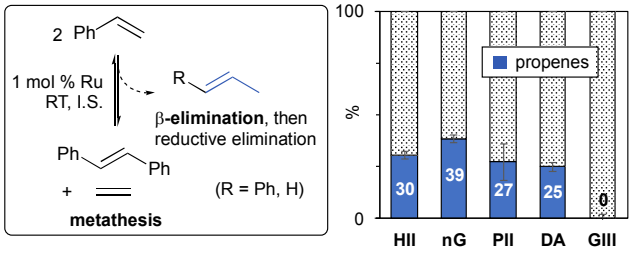

Figure 1. Quantifying the β-Elimination Pathway in Decomposition of Fast-Initiating Metathesis Catalysts: Propene Yields at Full Catalyst Decomposition. (Yields based on Ru precatalysts; reactions in C_6D_6 except for **PII**, for which solubility required use of CD_2Cl_2). I.S. = internal standard. See also Scheme 1b.

Examining Alternative Decomposition Pathways: Insight from the Nature of the Ru Products. The py ligands in **GIII** offer opportunities to trap the Ru products of decomposition. Of particular interest is the fate of the H_2IMes ligand in these products, as NHC activation and/or cyclometalation are common features in numerous potential pathways, including Buchner expansion (see below).[7] We therefore sought to identify the methyl-

idene-free Ru species formed on reaction of **GIII** with styrene. Scheme 3 depicts the major products observed under conditions corresponding to those of Figure 1: that is, the known tris-pyridine complex **Ru-3** (a known thermodynamic sink in this chemistry; see above),[8a] its bis-pyridine analog **Ru-3′**, and a new species assigned as ethylene adduct **Ru-4**.

Scheme 3. Bimolecular Decomposition of GIII During Olefin Metathesis in a Sealed System.[a]

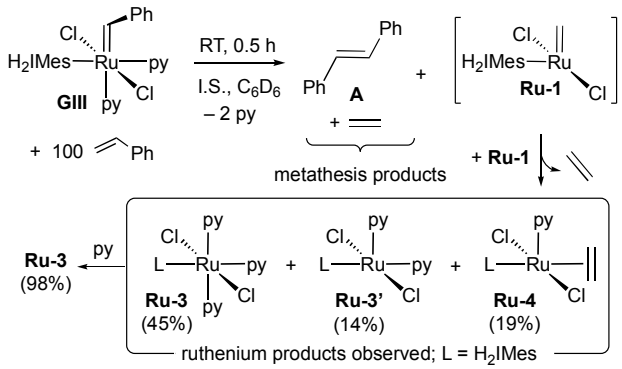

[a] Ethylene is generated by both metathesis of styrene, and methylidene coupling.

These sealed-tube reactions generate **Ru-3/3′** in ca. 60% yield, and **Ru-4** in ca. 20% yield based on ruthenium (Figure 2a; inverted spectrum). The presence of an ethylene ligand in **Ru-4** is supported by the observed transformation of this complex into **Ru-3′** when the solution is degassed to remove ethylene, and its reappearance when ethylene is reintroduced (Figure S13). Labile coordination of C_2H_4 is common in electron-rich Ru complexes.[8a,14,23] As further evidence for a weakly-bound ethylene ligand in **Ru-4**, the latter complex undergoes conversion to tris-py complex **Ru-3** when pyridine is added (as does bis-py complex **Ru-3′**). As shown in the upper NMR trace of Figure 2a, **Ru-3** is then the sole observable Ru species, being present in 98% yield based on starting **GIII**. As an indicator of generality, it should be noted that **Ru-3** is likewise observed for **HII** on successive treatment with styrene and pyridine, and (as discussed below) on decomposition of the methylidene and ethylidene complexes **GIIIm** and **GIIIe**.

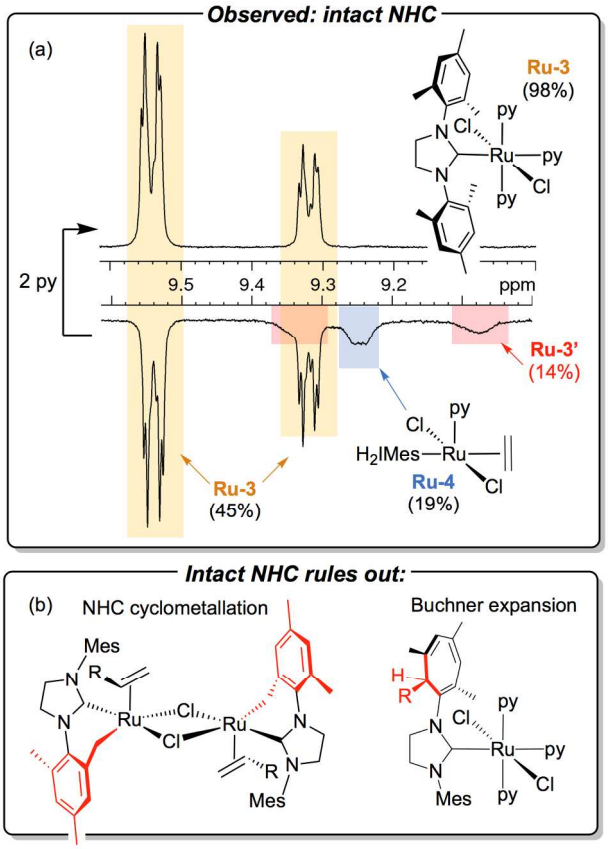

Figure 2. Ruthenium Decomposition Products: Identification and Mechanistic Implications. (a) ^{1}H NMR spectra corresponding to Scheme 3: diagnostic py *o*-C*H* region (C_6D_6, 300 MHz). Upper trace: **Ru-3**, formed by adding pyridine to (inverted trace) sample at full decomposition. For full spectra, see Fig. S13. (b) Decomposition pathways ruled out by quantitative formation of **Ru-3**.

A key structural feature in **Ru-3** is the intact H_2IMes ligand, which rules out decomposition processes that involve activation of H_2IMes. This precludes, for example, base-induced deprotonation of the metallacyclobutane, which would generate a Ru dimer containing a cyclometallated H_2IMes ligand[14] (Figure 2b, left) as well as "false" propenyl markers, as discussed above. The poor Brønsted basicity of pyridine[24] is a key parameter in inhibiting this pathway.

Also ruled out is pyridine-induced attack of the [Ru]=CHR carbon on a mesityl ring, which would give a cycloheptatriene product following Buchner expansion (Figure 2b, right).[25,26] Such transformations of **GII**, **HII**, and other Ru-H_2IMes catalysts were deliberately induced by Diver and co-workers, via reactions with CO or isonitriles.[25] Coordination of these π-acids heightens the electrophilicity of the Ru=CHR carbon, promoting cyclopropanation of a mesityl ring and ensuing ring expansion.[25,26a] Computational analysis by the Cavallo group suggested that pyridines are insufficiently π-acidic to cause Buchner expansion of benzylidene com-

plexes,[26] and the present studies bear out this prediction.[27]

Evidence for Bimolecular Coupling of [Ru]=CHR (R = Ph, Me). The foregoing demonstrates that several decomposition pathways known from other contexts are either inoperative, or less important than hitherto presumed. We next turned to establishing whether bimolecular coupling is operative. Unambiguous evidence for such coupling is seen for the benzylidene complex **GIII**. This precatalyst (in fact, typically a mixture of **GIII** and its mono-pyridine derivative **GIII'**; see below) eliminates stilbene **A** in up to 75% yield on prolonged heating at 60 °C (Scheme 4). The major Ru products are again **Ru-3** and its bis-pyridine analog **Ru-3'**, formed in up to 70% yield. Batch-to-batch variations in the proportions of these products (e.g., 1.5:1 to the reverse ratio) are not unexpected, given the known variability in the number of pyridine ligands present in the precatalyst[28,29] (a **GIII**–**GIII'** mixture, although exchange averaging results in observation of a single benzylidene peak by ^{1}H NMR analysis). Also observed, albeit as a minor product (invariably <5%), is $RuCl_2(py)_4$ **Ru-5**. Formation of the latter NHC-free complex indicates H_2IMes loss via a minor additional process as yet undetermined.[30]

Scheme 4. Representative Product Speciation on Thermal Decomposition of GIII.

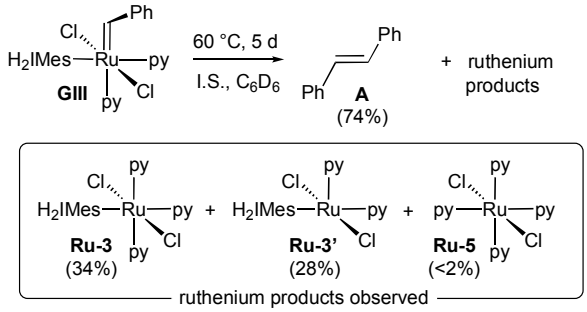

Ethylidene complex **GIIIe** (Scheme 5) decomposes dramatically faster than **GIII**. We were able to isolate **GIIIe** by stirring **GIII** under 1 atm cis-2-butene at the minimum accessible solution temperature in benzene, then lyophilizing the solvent to prevent premature decomposition upon concentrating. Heating a C_6D_6 solution of **GIIIe** and an internal standard at 60 °C causes loss of the alkylidene signal over 25 min, with evolution of up to 45% 2-butene. Also observed are propene and 2-pentene (24% each), indicating isomerization–metathesis of 2-butene. On adding pyridine, the Ru products again convert into **Ru-3** (85% yield, based on starting **GIIIe**).

Scheme 5. Synthesis and Bimolecular Decomposition of GIIIe.

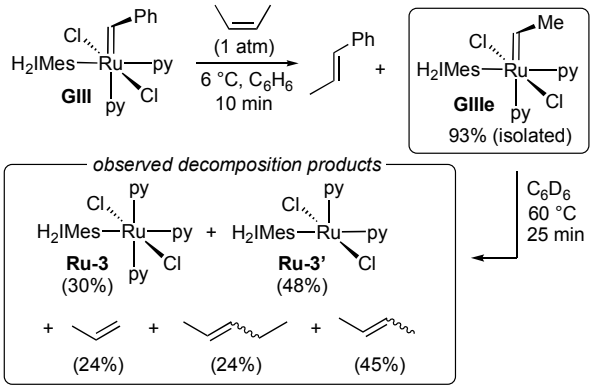

Evidence for Bimolecular Coupling of [Ru]=CH_2. While the observation of alkylidene coupling products in up to 75% yield for the benzylidene and ethylidene complexes is suggestive, the sterically unprotected methylidene ligand could be subject to additional reaction pathways. To clarify the decomposition behavior of methylidene intermediate **Ru-1**, we sought a weakly stabilized adduct that would permit direct study. No such complex is described in the literature. The sole isolable, metathesis-active Ru methylidene complexes reported to date are the "Grubbs methylidenes", i.e. **GIIm**[8,31] and its first-generation analog $RuCl_2(PCy_3)_2(=CH_2)$, **GIm**.[32a] Use of these complexes to probe bimolecular coupling is precluded by the low lability of the PCy_3 ligand[33] (which limits the concentration of **Ru-1** present at any given time), and by facile abstraction of the methylidene ligand as $[MePCy_3]Cl$,[8,9] as cited in the Introduction. As noted above, Hong and Grubbs attempted to synthesize the corresponding pyridine-stabilized species **GIIIm** via reaction of **GIII** with ethylene, but were unable to observe **GIIIm** even in situ.[8a] Few other Ru methylidene complexes are known, and these rare examples are not metathesis-active.[32]

Nevertheless, we envisaged that **Ru-1** might be successfully trapped by synthesizing the metallacyclobutane complex **Ru-2** in situ,[10] and introducing a stabilizing ancillary ligand to trigger retro-addition. While pyridine is an obvious candidate ligand, the literature reports emphasize its limited stabilizing ability.[8a,17] *o*-Dianiline (Scheme 6) offers an attractive alternative. This ancillary ligand, originally chosen to maximize catalyst productivity in ring-closing macrocyclization,[4] is similarly well-suited to stabilization of **Ru-1**. Design criteria common to both of these objectives include low nucleophilicity and low Brønsted basicity (essential to prevent ligand-mediated methylidene or proton abstraction, respectively).[9] Also critical is a balance between the coordinating properties required to *isolate* an adduct of **Ru-1**, vs. the lability required to readily *release* **Ru-1**. These conflicting demands are reconciled via a combination of good ligand donor ability (achieved, for *o*-dianiline, via a combination of donicity, steric accessibility at the nitrogen sites, and flexible chelation),[34] and high (hemi)lability.

Scheme 6. Synthesis of *o*-Dianiline Adduct Ru-6.[a]

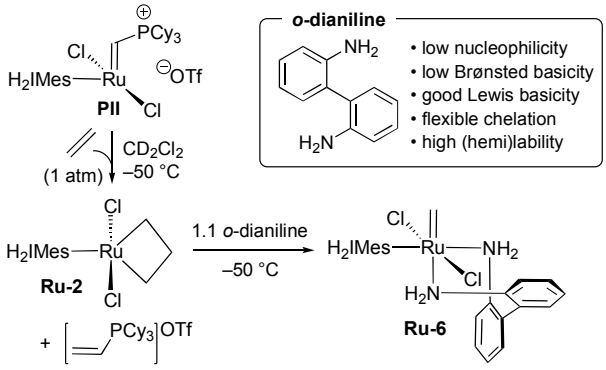

[a] Isolated by precipitating with pentane at –78 °C.

*Synthesis of Transiently-Stabilized Methylidene Adducts of **Ru-1***. In initial NMR-tube experiments (Scheme 6), a solution of **PII** in CD_2Cl_2 was freeze-thaw degassed, thawed at –50 °C, and exposed to ethylene. A color change from brown to dark pink occurred within 5 min, with clean conversion to **Ru-2** (Figure 3, top trace). Slow injection of *o*-dianiline in CD_2Cl_2 caused a further color change to green over the next 0.5 h, with loss of the diagnostic upfield signal for the metallacycle (H_β; –2.6 ppm), and emergence of the methylidene singlet for **Ru-6** (19.3 ppm; Figure 3, inverted trace). The diagnostic, formally diastereotopic NH_2 signals for bound *o*-dianiline appear as two broad, unresolved signals at ca. 3.6 and 4.3 ppm. Their assignment was confirmed by injecting D_2O into the cooled solution, and briefly agitating to dissolve the ice. In situ yields of **Ru-6** were quantitative. To isolate **Ru-6** free of reagent ethylene, the reaction was repeated on 75 mg scale, and **Ru-6** was isolated as a pale green solid in 75% yield by precipitating with a trickle of cold pentane at –78 °C.

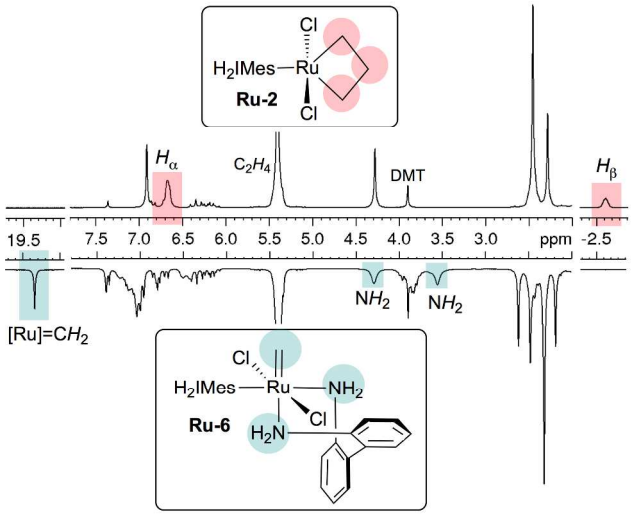

Figure 3. ^{1}H NMR spectra showing (top) **Ru-2**, and (inverted) its *o*-dianiline-stabilized derivative **Ru-6** (300 MHz, CD_2Cl_2, –50 °C). Diagnostic NMR signals for **Ru-2** and **Ru-6** are highlighted with bars that approximate the colours of the complexes.

The corresponding experiments with **GIIIm**, synthesized by adding 2 equiv py (Scheme 7), afforded a mixture of **GIIIm** and its mono-pyridine derivative **GIIIm'**. These species were generated in a 30:70 ratio, as determined by integration of the two distinct methylidene signals (19.35 and 18.63 ppm, respectively) at –50 °C. The higher lability of the monodentate pyridine ligand renders these complexes much more unstable than **Ru-6**, and considerably more challenging to isolate. However, they were successfully obtained by carrying out pyridine addition at –78 °C to form **GIIIm/m'**, and precipitating the product mixture by cannula addition of cold pentane at ca. –120 °C. Even under these conditions, competing decomposition (loss of ethylene) was evident. Nonetheless, the methylidene products were isolated as a yellow solid, in ca. 60% yield based on starting **PII**, by decanting the pentane and drying in vacuo. Their stability was insufficient to withstand washing, even in the solid state.

Scheme 7. Synthesis of Pyridine-Stabilized GIIIm/m'.[a]

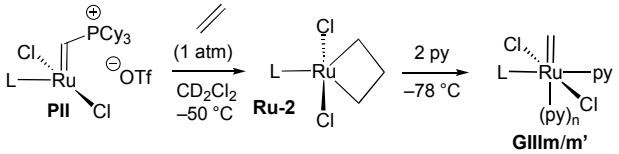

[a] **GIIIm:** n = 1; **GIIIm'**: n = 0; L = H_2IMes. The 30:70 mixture was precipitated with pentane at –116 °C. The vinylphosphonium coproduct in step 1 is omitted for clarity.

Evidence for Bimolecular Coupling of Transiently-Stabilized Methylidene Species. To measure the proportion of ethylene released by coupling of dianiline adduct **Ru-6**, this complex was dissolved in cold CD_2Cl_2 and added to the internal standard in a pre-chilled J. Young tube. The temperature was maintained at –20 °C during sample preparation by use of a sand-bath chilled in the glovebox freezer. Warming to RT resulted in 95% decomposition over 75 min (Figure 4), and formation of methylidene-free **Ru-7** in up to 90% yield. Only 30% yield of ethylene was detected, however, owing to volatilization into the headspace. The proportion of ethylene detected increased to ca. 65% when **Ru-6** was permitted to decompose in NMR tubes filled to 80% capacity. This constitutes the minimum headspace volume deemed safe to prevent explosion on warming (for calculations, see SI).

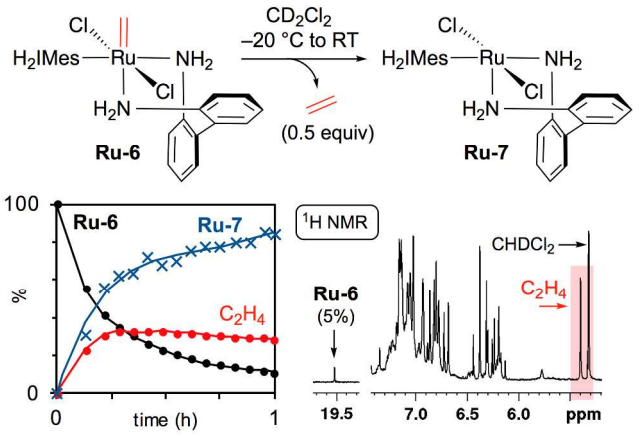

Figure 4. Bimolecular coupling of **Ru-6**: rate curve and ^{1}H NMR spectrum (300 MHz, CD_2Cl_2, RT) at 95% decomposition.

In these filled-tube experiments, the yield of the Ru decomposition product **Ru-7** dropped to ca. 65%, probably owing to the improved stability of Ru-C_2H_4 adducts (cf. **Ru-4**) at higher solution concentrations of ethylene. New ^{1}H NMR signals were indeed observed in the region characteristic of the Ru-bound C_2H_4 ligand (3.5–0.9 ppm),[14,23] as well as the N*H* region (5.0–3.4) for Ru-dianiline complexes, although the lability of bound ethylene in these complexes precludes isolation.

The corresponding experiments with the pyridine adducts **GIIIm/m'** resulted in complete decomposition within 20 min, consistent with the high lability of the pyridine ligands noted. Higher proportions of ethylene were detected (76% in $CDCl_3$; 70% in CD_2Cl_2), probably because mass transfer restrictions in the NMR tube retard partitioning of ethylene into the gas phase over this short reaction time. Bimolecular coupling is thus observed for both of these exemplary class B/C catalysts, although the weaker donor ligands characteristic of Class C accelerate decomposition.

Dependence of the Rate of Bimolecular Coupling on Alkylidene Substituent. The data above support bimolecular decomposition of all [Ru]=CHR complexes examined, at rates that are qualitatively found to increase as the bulk of the substituent R decreases. This behaviour, which parallels trends observed in the early-metal systems, is shown more explicitly in Figure 5. Thus, after 30 min at 60 °C in C_6D_6, benzylidene complex **GIII** remains intact, while its ethylidene or methylidene analogues (**GIIIe** and **GIIIm**, respectively) are completely decomposed. A striking difference between **GIIIe** and **GIIIm** is evident at room temperature, however. After 30 min in CD_2Cl_2, 99% **GIIIe** remains, while **GIIIm/m'** is completely decomposed. The greater resistance to coupling of the ethylidene complex **GIIIe** helps account for the widely-reported[35-37] observation of improved metathesis performance for 2-methyl olefins, vs 1-olefins.[38]

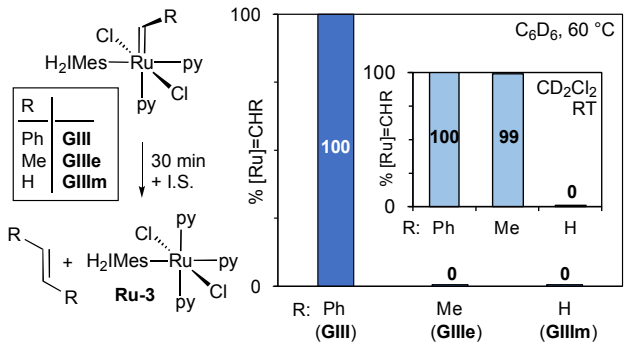

Figure 5. Bimolecular coupling of [Ru]=CHR: impact of R on rate of decomposition. Chart shows % alkylidene remaining after 30 min at 60 °C, or (inset) at RT, for **GIII**, **GIIIe**, and **GIIIm**. All complexes shown as bis-py species for simplicity: in practice, a mixture of mono- and bis-py complexes is present (of which the latter predominates for all but **GIIIm/m'**).

Mechanism of Bimolecular Coupling. To gain further insight into the mechanism of bimolecular coupling, we undertook kinetics and computational analysis.

Kinetics studies. Rate experiments focused on dianiline adduct **Ru-6**, given its greater ease of handling relative to **GIIIm**. At 20 mM **Ru-6**, decomposition was second-order in Ru, consistent with rate-limiting bimolecular coupling of five-coordinate **A** (Figure 6a). At 1 mM **Ru-6**, decomposition is *first* order in Ru, but the evolution of ethylene confirms that bimolecular coupling remains operative. Indeed, the observed yield of C_2H_4 reached ca. 40% based on starting **Ru-6**, despite use of a standard NMR-tube headspace to maintain conditions that more closely approximate bench operations. Volatilization of ethylene is limited by the small amounts involved (maximum theoretical yield 0.5 mM, well below its reported solubility limit of 54 ±3 mM in CD_2Cl_2 at 296 ±1.5 K).[9d]

Decomposition at 1 mM is also found to be retarded by exogenous dianiline. This, and the change in the order of reaction with respect to [**Ru-6**], point toward a change in mechanism when the ruthenium concentration is decreased. The rate of coupling of five-coordinate **A** (path a) is expected to be highly sensitive to concentration, given its squared dependence on [**Ru-6**]. We propose that at 1 mM **Ru-6**, loss of dianiline from **A** (path b) is faster than coupling of **A**. Once four-coordinate **Ru-1** is generated, its greatly reduced steric protection relative to **A** is expected to result in a significantly faster rate in the bimolecular coupling step (that is, $k_4 >> k_2$).

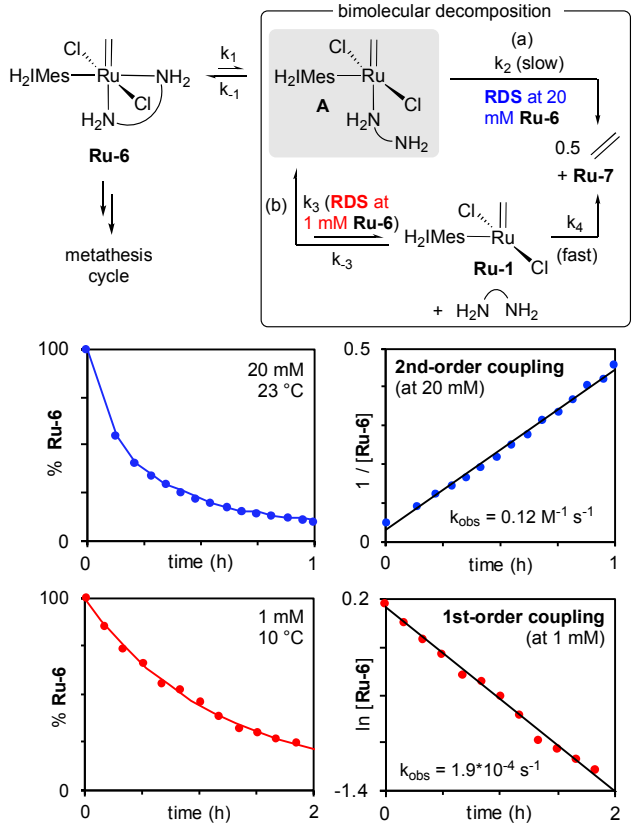

Figure 6. Top: Proposed mechanism for bimolecular coupling at (a) 20 mM **Ru-6**; (b) 1 mM **Ru-6**. (Reactions in CD_2Cl_2; $H_2N–NH_2$ = *o*-dianiline). Bottom: Establishing the order of reaction with respect to Ru. To retard reaction and collect sufficient scans for good signal-to-noise ratios, the 1 mM reaction was conducted at 10 °C.

Molecular-Level Computational Studies. DFT analysis focused on coupling of **Ru-1**. This species was chosen for study in light of the kinetics findings above, which point toward **Ru-1** as the key intermediate in decomposition at catalytically relevant concentrations of **Ru-6**. In addition, **Ru-1** is common to all of the Class B/C catalysts studied in this work, including those which (subsequent to initiation) lack a ligand that can stabilize the methylidene intermediate.

Accordingly, the mechanism by which two molecules of **Ru-1** couple to generate ethylene was examined. The dimeric structures shown at the left in Figure 7 were prioritized in light of prior experimental and computational work suggesting their potential importance.[6,16,39,40] The energies shown for these structures are normalized to that of **Ru-6**. Dimer **Ru-10** has multiple precedents in crystal structures of diruthenium species containing transoid alkylidene ligands.[41] **Ru-10** is the lowest-energy of the intermediates predicted to form on reaction of two **Ru-1** molecules. However, the long $H_2C\cdots CH_2$ distance (5.77 Å), and the substantial rearrangement needed for the two methylidene units to react, imply that this intermediate cannot generate ethylene in a single elementary step.

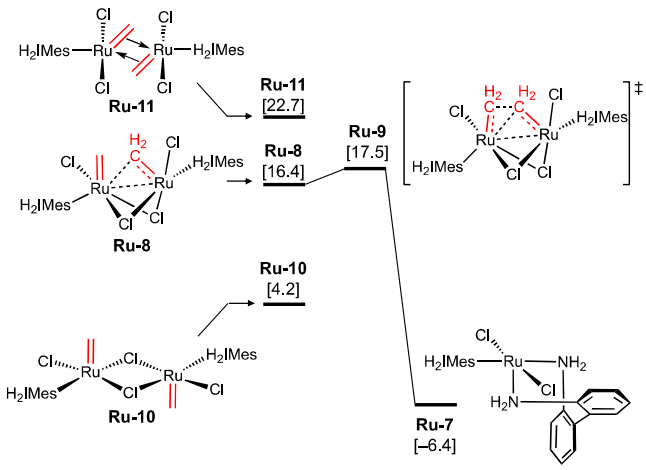

Figure 7. Computed Gibbs free energy profile (kcal/mol) along the reaction path involving loss of methylidene from **Ru-1**. Energies normalized to *o*-dianiline adduct **Ru-6**.

Considerably higher in energy than **Ru-10** is **Ru-11**, precedent for which exists in a crystallographically characterized tungsten methylidene complex that exhibits reciprocal methylidene-to-tungsten donor interactions.[19c] Shown in the structure of **Ru-11** is the corresponding reciprocal $Ru{=}CH_2{\rightarrow}Ru$ donation. Although the two methylidene units are closer in **Ru-11** than they are in **Ru-10**, they are geometrically constrained and cannot easily interact. Attempts to enforce coupling by shortening the C–C distance to form an ethylene ligand between the two Ru centers required unacceptably high energies, >35 kcal/mol higher than **Ru-6**, and a transition state was therefore not located.

Much more persuasive as an intermediate on the methylidene-coupling pathway is **Ru-8**, which is higher in energy than **Ru-10**, but lower than **Ru-11**. In structure **Ru-8**, the two $Ru{=}CH_2$ units form a cisoid dimer in which the methylidene carbons are sufficiently close and unconstrained to interact (2.90 Å; for 3D structure, see Figure S5). Also notable is a striking dissymmetry in the methylidene bonding interactions. While the calculated $Ru{=}CH_2$ bond distances are essentially identical, at 1.82 or 1.83 Å, one methylidene ligand interacts with both metal centers, while the other does not ($Ru_A–C_B$ = 2.64 Å; $Ru_B–C_A$ = 3.67 Å; for atom labeling, see Figure 8). Most importantly, the orientation of the methylidene groups of **Ru-8** is optimal for C–C bond formation. Less than 2 kcal/mol is needed to reach transition state **Ru-9** (the 3D structure of which is shown in Figure S6), and these two stationary points have been connected in intrinsic reaction coordinate (IRC) calculations. A related $Ru_2(\mu\text{-}Cl)_2$ transition state was identified in a recent DFT study focusing on the formation of alkylidenes $RuCl_2(H_2IMes)(=CRR')$ in the reaction of $RuCl_2(H_2IMes)$

with olefin.[16] The relatively low energy required to reach transition state **Ru-9** (<20 kcal/mol above **Ru-6**) underscores the ease of bimolecular coupling. Ensuing loss of ethylene and trapping by free dianiline affords the methylidene-free product **Ru-7**.

To clarify the orbital interactions that lead to coupling of two molecules of **Ru-1**, we undertook natural bond orbital (NBO) analysis[42] of intermediate **Ru-8** (Figure 8). This analysis suggests that coupling is enabled by two principal orbital interactions. First, electron density is donated from the filled π orbital on Ru_B=C_B into an empty orbital on Ru_A (Figure 8a). This interaction establishes a small, shared electron population between Ru_A and C_B, and between the two Ru atoms (Wiberg index[43] 0.14 in each case; Table S7). Secondly, as shown in Figure 8b, back-donation of electron density from the filled π orbital on Ru_A=C_A into the π* orbital on Ru_B=C_B causes buildup of electron density between C_A and C_B. This interaction is strengthened by polarization of the Ru_B=C_B π bond towards Ru_B, which results in polarization of the corresponding π* orbital in the opposite direction. C→Ru polarization of the alkylidene bond is consistent with the experimentally-observed electrophilicity of the [Ru]=CHR carbon.[8,9] Previous computational studies,[44] as well as the present work (Tables S8, S9), indicate that this polarization is essentially limited to the π-component of the bond.

NBO analysis of the ensuing transition state **Ru-9** reveals the expected enhancement of the two orbital interactions discussed for **Ru-8**. Nevertheless, the shared electron density between the C_A and C_B is low even in **Ru-9** (Wiberg index[43] of 0.27), indicating that most of the C–C bond is formed subsequent to this transition state.

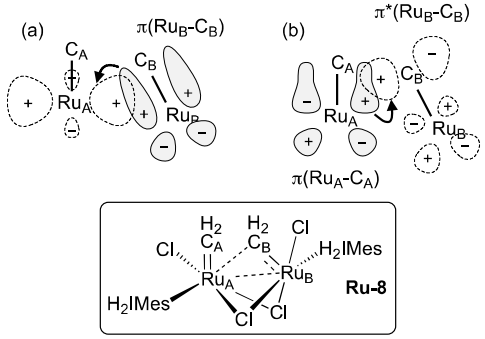

Figure 8. Key orbital interactions for Ru-methylidene coupling and C–C bond formation. Dashed lines signify unoccupied orbitals. Charge flow (donation) is indicated by arrows. Atom labeling in intermediate **Ru-8** shown in box.

CONCLUSIONS

Fast initiation has long been connected to fast decomposition in Ru-catalyzed olefin metathesis. Prior studies of highly active, fast-initiating Ru-NHC catalysts identified elimination of propene from the unsubstituted metallacyclobutane as central to decomposition. Bimolecular coupling, in contrast, has been viewed as largely irrelevant for the highly active Ru-NHC catalysts. The foregoing corrects this perspective. Bimolecular coupling can now be recognized as an important contributor to decomposition of fast-initiating ruthenium metathesis catalysts. Improved activity – in particular, higher initiation efficiency – has long been a major focus of catalyst design efforts in Ru-catalyzed metathesis. The present work suggests that such efforts may be undermined by accelerated decomposition. Further, it highlights the importance of inhibiting bimolecular elimination of the methylidene ligand in designing new metathesis catalysts or reaction protocols.

EXPERIMENTAL AND COMPUTATIONAL SECTION

General Procedures. Reactions were carried out under N_2 in a glovebox or on a Schlenk line. Dichloromethane, benzene, and hexanes were dried and degassed using a Glass Contour solvent purification system. Pentane was distilled over $MgSO_4$, then P_2O_5. C_6D_6 and $CDCl_3$ (Cambridge Isotopes) were degassed by five consecutive freeze/pump/thaw cycles. CD_2Cl_2 (Cambridge Isotopes) was received in sealed ampoules packed under N_2. All solvents were stored under N_2 over 4 Å molecular sieves for at least 16 h prior to use. Styrene (Aldrich, 99%), methyl 10-undecenoate (Aldrich, 96%), and D_2O (Cambridge Isotopes) were degassed by five consecutive freeze/pump/thaw cycles, and stored under N_2 at –35 °C. Dimethyl terephthalate (DMT: Aldrich, 99%), trimethoxybenzene (TMB: Aldrich, 99%), anthracene (Aldrich, 97%), pyridine (anhydrous; Aldrich, 99.8%), ethylene (BOC Ultra-High Purity grade 3.0, 99.9%; Linde), and cis-2-butene (Lab Network Inc, 99%) were used as received. *o*-Dianiline ([1,1'-biphenyl]-2,2'-diamine)[45] $RuCl_2(py)_4$,[46] **GIII**,[28] **HII**,[47] **DA**,[4] and **PII** (as the trifluoromethanesulfonate salt)[48] were prepared via literature procedures.

NMR spectra were recorded on an Avance 300, Avance II 300, or Avance III 600 cryoprobe NMR spectrometer, at 23 ±2 °C except where otherwise indicated. Chemical shifts are reported in ppm, and referenced against the residual proton or carbon signals of the deuterated solvents (^1H, ^{13}C). Overlapping ^1H NMR integrations were deconvoluted using the "deconvolve and display" function in Topspin (NMR processing software; v3.5 pl 5). Oxygen and moisture were excluded from air-sensitive samples using either screw-capped NMR tubes (equipped with PTFE septa, where *o*-dianiline solutions were to be injected) or 3 mm valved J. Young NMR tubes (Figure S1). Infrared (IR) spectra were recorded on a Thermo Scientific Nicolet 6700 Fourier Transform IR spectrometer equipped with a Smart iTR Attenuated Total Reflectance (ATR) sampling accessory. GC-MS

analysis was performed using an Agilent 5975B inert XL EI/Cl instrument equipped with a polysiloxane column. Anaerobic MALDI mass spectra were collected on a Bruker UltrafleXtreme MALDI-TOF/TOF mass spectrometer interfaced to a glovebox. Samples were calibrated internally using the peaks for pyrene (*m*/*z* 202.0783) and $[H_2IMes•H]^+$ (*m*/*z* 307.2174).

Quantification of propenyl species formed during styrene metathesis. To maximize retention of propene, these experiments were conducted in filled J. Young NMR tubes. A small headspace (0.15 mL; ca. 5% of the tube volume) was provided to accommodate any unintended thermal expansion of the solvent in these nominally isothermal (23 °C) experiments.

In a representative reaction, a capillary tube was inserted into a J. Young NMR tube as a mechanical aid to mixing. A solution of **HII** (24 mg, 0.038 mmol) and anthracene (ca. 3 mg; internal standard) in 1.46 mL C_6D_6 was added, and a ^{1}H NMR spectrum was measured to establish the starting ratio of **HII** vs anthracene. Styrene (440 μL, 3.8 mmol, 100 equiv) was then added, and the tube was inverted several times to mix the solution. Subsequent controlled mixing was accomplished by attaching the tube to a rotary evaporator, and setting it to rotate at ca. 15 rpm (Figure S2). Falling of the internal capillary with every inversion of the tube effects equilibration, and enables accurate, reproducible quantitation. A color change from green to brown occurred, followed by precipitation of a dark green solid over 1 h. Complete loss of **HII** was evident at this point. ^{1}H NMR (C_6D_6, 300 MHz; diagnostic signals only; Figure S11): δ 16.72 (s, 1H, [Ru]=C*H*Ar of **HII**; none remaining), 8.19 (s, 2H, Ar C*H* of anthracene), 7.00 (s, 2H, =C*H* of stilbene), 6.58 (dd, $^3J_{HH}$ = 18 Hz, $^3J_{HH}$ = 11 Hz, =C*H*Ph of styrene), 6.19 (dt, $^3J_{HH}$ = 16 Hz, $^3J_{HH}$ = 7 Hz, 1H, =C*H*CH_2Ph of 1,3-diphenylpropene;[15] not observed), 6.03 (dq, $^3J_{HH}$ = 15.9 Hz, $^3J_{HH}$ = 6.8 Hz, 1H, =C*H*CH_3 of β-methylstyrene;[15] 12%), 5.27 (s, C_2H_4), 5.01–4.92 (m, three-quarters of the propene =CH_2 pattern;[49] the remaining multiplet is partially obscured by signal for excess styrene; 18%). The corresponding propenes arising from elimination of the isopropoxyphenyl-substituted metallacyclobutane[15] were not observed, perhaps reflecting the large excess of styrene present in solution. Adding 4 equiv pyridine to the reaction results in slow dissolution of the green solid, and a colour change to from green to orange. After 24 h: ^{1}H NMR (C_6D_6, 300 MHz; diagnostic signals only): δ 9.62 (dt, $^3J_{HH}$ = 5.2 Hz, $^4J_{HH}$ = 1.5 Hz, 4H, py *o*-C*H* **of Ru-3**, 78%).

Identification of Ru species formed on metathesis of styrene by GIII. In a representative experiment, a solution of **GIII** (7.3 mg, 0.010 mmol) and anthracene (ca. 1 mg; internal standard) in 385 μL C_6D_6 was added to a J. Young NMR tube. A ^{1}H NMR spectrum was measured to establish the starting ratio of **GIII** vs anthracene, and styrene (115 μL, 1.0 mmol, 100 equiv) was then added. A colour change from green to orange was observed within the first 30 min, followed by a change back to green. No signals for **GIII** or other [Ru]=CHR species were evident after 35 min: ^{1}H NMR (C_6D_6, 300 MHz; diagnostic signals only; Figure S12): δ 19.66 (s, 1H, [Ru]=C*H*Ph of **GIII**; none remaining), 9.62 (dt, $^3J_{HH}$ = 5.2 Hz, $^4J_{HH}$ = 1.5 Hz, 4H, py *o*-C*H* **of Ru-3**, 45%), 9.25 (br d, 2H, py *o*-C*H* of **Ru-4**, 19%), 9.16 (br s, 2H, py *o*-C*H* of **Ru-3′**, 14%), 8.19 (s, 2H, C*H* of anthracene). Adding pyridine (5 μL, 6 equiv) effected immediate conversion to **Ru-3** as the sole py species present (98% yield).

^{1}H NMR data for the individual complexes are given below.

$RuCl_2(H_2IMes)(py)_3$ Ru-3: ^{1}H NMR (C_6D_6, 300 MHz; Figure S15): δ 9.62 (dt, $^3J_{HH}$ = 5.2 Hz, $^4J_{HH}$ = 1.5 Hz, 4H, py *o*-C*H*), 9.39 (dt, $^3J_{HH}$ = 4.9 Hz, $^4J_{HH}$ = 1.6 Hz, 2H, py *o*-C*H*), 6.53 (tt, $^3J_{HH}$ = 7.5 Hz, $^4J_{HH}$ = 1.6 Hz, 1H, py *p*-C*H*), 6.41 (tt, $^3J_{HH}$ = 7.4 Hz, $^4J_{HH}$ = 1.5 Hz, 2H, py *p*-C*H*), 6.28 (m, 2H, py *m*-C*H*; overlaps with Mes C*H*), 6.28 (s, 4H, Mes C*H*; overlaps with py *m*-C*H*), 5.98 (m, 4H, py *m*-C*H*), 3.64 (s, 4H, NCH_2), 2.77 (s, 12H, *o*-CH_3), 1.88 (s, 6H, *p*-CH_3). Values in CD_2Cl_2 are in excellent agreement with those reported in the same solvent.[8a]

$RuCl_2(H_2IMes)(py)_2$ Ru-3′: ^{1}H NMR (C_6D_6, 300 MHz; Figures S15): δ 9.42 (br s, 2H, py *o*-C*H*; overlaps with py *o*-C*H* of **Ru-3**), 9.15 (br s, 2H, py *o*-C*H*), 6.67–6.35 (br s, 6H, Mes C*H* and py C*H*; overlaps with py *m*/*p*-C*H* of **Ru-3**), 6.28 (s, 2H, Mes C*H*; overlaps with Mes C*H* of **Ru-3**), 6.03 (br s, 2H, py *m*-C*H*; overlaps with py *m*-C*H* of **Ru-3**), 3.48 (br s, 4H, NCH_2), 2.75 (br s, 12H, o-CH_3), 1.99 (br s, 6H, *p*-CH_3). ^{1}H NMR (CD_2Cl_2, 300 MHz): δ 8.94 (br s, 2H, py *o*-C*H*), 8.60 (br s, 2H, py *o*-C*H*), 7.51 (br s, 1H, py *p*-C*H*), 7.25 (s, 1H, py *p*-C*H*), 7.00 (br s, 2H, py *m*-C*H*), 6.59 (br s, 2H, py *m*-C*H*), 6.34 (s, 4H, Mes C*H*), 3.97 (s, 4H, NCH_2), 2.48 (s, 12H, *o*-CH_3), 2.15 (s, 6H, *p*-CH_3). All ^{1}H NMR signals for **Ru-3′** are broad ($\omega_{1/2}$ ~5–50 Hz) at RT, indicating fluxionality. A monomeric formulation is supported by DOSY-NMR analysis, which shows slightly faster diffusion for **Ru-3′** than **Ru-3**. Key ^{13}C NMR signals (located by ^{1}H–^{13}C HMQC; C_6D_6, 300 MHz): 154.0 (py *o*-CH), 152.6 (py *o*-CH), 121.7 (py *m*-CH), 52.4 (NCH_2), 20.6 (Mes *p*-CH_3), 19.2 (Mes *o*-CH_3).

$RuCl(H_2IMes)(C_2H_4)(py)$ Ru-4: ^{1}H NMR (C_6D_6, 300 MHz; Figure S12): δ 9.30 (br d, $^3J_{HH}$ = 5.3 Hz, 2H, py *o*-C*H*), 6.63 (py *m*-CH; overlaps with styrene =C*H*; 2D-detected via COSY), 3.59 (br s, 4H, NCH_2), 3.05 (br s, 3H, Mes CH_3), 2.67 (br s, 3H, Mes CH_3), 2.49 (br s, 6H, Mes CH_3), 2.11 (br s, 3H, Mes CH_3), 1.70 (br s, 3H, Mes CH_3). Signals for Mes C*H*, py p-C*H*, and C_2H_4 are masked by overlap with **Ru-3/3′** and styrene. ^{1}H–^{1}H NOESY: δ 9.30 (py *o*-C*H*) and 6.63 (py *m*-C*H*), 9.30 and 2.67 (Mes CH_3). Stirring a mixture of **Ru-3/3′/4** in C_6D_6 at RT under N_2 for 3 h resulted in a colour change from green to orange, and complete consumption of **Ru-4** (Figure S13). At t_0:

45% **Ru-3**, 19% **Ru-3′**, 34% **Ru-4**. After 3 h: 22% **Ru-3**, 66% **Ru-3′**, 0% **Ru-4**; 11% missing Ru. Adding ethylene (1 atm) resulted in reformation of **Ru-4**. After ethylene addition: 51% **Ru-3**, 4% **Ru-3′**, 29% **Ru-4**; 16% missing Ru.

Bimolecular Coupling of GIII. In a representative reaction, solid **GIII** (9.6 mg, 0.013 mmol) and ca. 1 mg DMT were dissolved in 0.66 mL C_6D_6 in a J. Young NMR tube, to give a final Ru concentration of 20 mM. A ^{1}H NMR spectrum was recorded to establish the initial integration ratio of **GIII** relative to DMT. The NMR tube was heated to 60 °C in a thermostatted oil bath, and decomposition of **GIII** was monitored by ^{1}H NMR analysis over 5 d, during which time the color changed from green to orange. After this time, no **GIII** remained. ^{1}H NMR (C_6D_6, 300 MHz; diagnostic signals; Figures S14, S15): δ 19.66 (s, 1H, [Ru]=C*H*Ph of **GIII**; none remaining), 9.62 (dt, $^3J_{HH}$ = 5.2 Hz, $^4J_{HH}$ = 1.5 Hz, 4H, py *o*-C*H* of **Ru-3**; 34%), 9.16 (br d, $^3J_{HH}$ = 4.2 Hz, 2H, py *o*-C*H* of **Ru-3′**; 28%), 9.06 (dt, $^3J_{HH}$ = 5 Hz, $^4J_{HH}$ = 1.5 Hz, 8H, py *o*-C*H* of **Ru-4**; 1.6%), 8.00 (s, 4H, C*H* of DMT), 7.33 (m, 4H, *o*-C*H* of *(E)*-stilbene; 74%), 7.24 (m, 4H, *o*-C*H* of *(Z)*-stilbene; none present).

(E)-PhCH=CHPh: ^{1}H NMR (C_6D_6, 300 MHz): δ 7.33 (m, 4H, *o*-C*H*), 7.17 (m, 4H, *m*-C*H*), 7.08 (m, 2H, *p*-C*H*), 7.01 (s, 2H, =C*H*). EI MS, *m*/*z*: [M$^+$] 180.1 (simulated: 180.1 for $C_{14}H_{12}$). The ^{1}H NMR and GC-MS data matched those of a commercial sample (Sigma-Aldrich).

(Z)-PhCH=CHPh (Alfa Aesar, not observed): ^{1}H NMR (C_6D_6, 300 MHz): δ_H 7.24 (m, 4H, *o*-C*H*), 7.06–6.93 (m, 6H, *m*- and *p*-C*H*), 6.47 (s, 2H, =C*H*).

Synthesis of $RuCl_2(H_2IMes)(py)_2(=CHMe)$, GIIIe. Synthesis of **GIIIe** was carried out by a modified version of the method reported[17] for the 3-bromopyridine analog. Decomposition of **GIIIe** was minimized by performing the reaction in C_6H_6 at near-freezing temperatures, and then subliming the solvent by freeze-drying. On the Schlenk line, a solution of **GIII** (100 mg, 0.138 mmol) in C_6H_6 (2 mL) was freeze/pump/thaw degassed, then thawed at 6 °C. Cis-2-butene (1 atm) was admitted via the side-arm of the Schlenk flask, and the reaction was stirred for 10 min, over which time it turned from green to brown, and a red-brown solid precipitated. Pyridine (100 μL) was then injected, and the solution was frozen and lyophilized. The resulting tan powder was suspended in pentane (2 mL) in the glovebox, filtered, washed with pentane (3 x 1 mL), and dried in vacuo. Repeating the entire process with the crude product afforded **GIIIe** as a reddish-tan powder (85 mg, 93%), containing trace **Ru-3** and **GIII** (each ≤1%). Re-subjecting to reaction with butene, or reprecipitating from CH_2Cl_2–pentane at 0 °C, led to competing decomposition. **GIIIe** is sufficiently stable to observe at RT by ^{1}H NMR spectroscopy, but its spectrum degrades noticeably over the longer collection times required for ^{13}C NMR analysis (3-4 h).

^{1}H NMR (C_6D_6, 300 MHz, Figure S16): δ 19.53 (q, $^3J_{HH}$ = 5.9 Hz, [Ru]=C*H*Me), 8.64 (br s, 4H, py *o*-C*H*), 6.78 (s, 2H, Mes C*H*), 6.75 (s, 2H, Mes C*H*), 6.71 (br s, 2H, py *p*-C*H*), 6.42 (br s, 4H, py *m*-C*H*), 3.50–3.37 (m, 2H, NCH_2), 3.37–3.23 (m, 2H, NCH_2), 2.78 (s, 6H, Mes CH_3), 2.57 (s, 6H, Mes CH_3), 2.11 (br s, 3H, Mes CH_3), 2.10 (d, $^3J_{HH}$ = 5.9 Hz, 3H, [Ru]=CHCH_3; overlaps with Mes CH_3), 2.06 (br s, 3H, Mes CH_3).

^{1}H NMR ($CDCl_3$, 300 MHz, –20 °C): δ 19.10 (br q, $^3J_{HH}$ = 5.7 Hz, [Ru]=C*H*Me), 8.70 (br d, $^3J_{HH}$ = 3.7 Hz, 2H, py *o*-C*H*), 8.06 (br s, 2H, py *o*-C*H*), 7.52 (br t, $^3J_{HH}$ = 7.5 Hz, 1H, py *p*-C*H*), 7.43 (br t, $^3J_{HH}$ = 6.6 Hz, 1H, py *p*-C*H*), 7.06 (br s, 2H, py *m*-C*H*), 6.96 (br s, 4H, Mes C*H*), 6.79 (br s, 2H, py *m*-C*H*), 4.20–4.02 (m, 2H, NCH_2), 4.04–3.87 (m, 2H, NCH_2), 2.55 (s, 6H, Mes CH_3), 2.42 (s, 6H, Mes CH_3), 2.32 (br s, 3H, Mes CH_3), 2.21 (br s, 3H, Mes CH_3), 1.72 (d, $^3J_{HH}$ = 5.7 Hz, [Ru]=CHCH_3, 3H).

^{13}C{^{1}H} NMR ($CDCl_3$, 300 MHz, –20 °C; Figure S18): δ 330.1 ([Ru]=CHMe; ^{1}H-detected via HSQC), 219.4 (C_{NHC}), 150.8 (py *o*-CH), 149.9 (py *o*-CH), 139.0, 138.5, 138.1, 137.9, 136.4, 136.2 (py *p*-CH), 135.0 (py *p*-CH), 129.2 (Mes *C*H), 128.9 (py *m*-CH), 128.2, 123.5 (Mes *C*H), 123.2 (py *m*-CH), 51.0 (NCH$_2$), 50.7 (NCH$_2$), 46.4 ([Ru]=CHCH$_3$), 21.1 (Mes *C*H$_3$), 20.9 (Mes *C*H$_3$), 19.7 (Mes *C*H$_3$), 18.5 (Mes *C*H$_3$). IR (ATR, cm^{-1}): ν(C–H) 2864 (w), ν(CH$_3$) 1484 (m), ν(CH$_3$) 1405. MALDI-TOF MS (pyrene matrix), *m*/*z*: [RuCl(H$_2$IMes)(pyrene)]$^{\bullet+}$ 645.12 (42%; calc'd: 645.16), [Ru(H$_2$IMes–H)(pyrene)]$^{\bullet+}$ 609.14 (67%; calc'd: 609.18), [RuCl(H$_2$IMes–H)]$^{\bullet+}$ 442.05 (100%; calc'd: 442.08). Sample decomposition precluded satisfactory microanalysis.

Bimolecular Coupling of GIIIe: Quantification of Butene and Ru-3/3′. *Caution!* Thermal expansion in these variable-temperature experiments results in an explosion hazard, because it is essential to minimize the headspace in the NMR tube in order to measure as much as possible of the volatile products evolved (e.g., propene, butene). To minimize this risk, the headspace volume required to accommodate thermal expansion of the solvent and evolution of butene was calculated (see SI), and quadrupled to provide a safety margin. Any potential for damage to personnel or the NMR probe was limited further by warming the sample only behind a blast shield (not in the probe), and using a face shield when transferring the tube to and from the NMR probe.

In a representative experiment, a solution of **GIIIe** (13.9 mg, 0.0209 mmol) and DMT (ca. 1 mg) in C_6D_6 (2.75 mL) was added to a J. Young tube. A ^{1}H NMR spectrum was recorded to establish the initial integration ratio of **GIIIe** relative to DMT. The full length of the NMR tube was heated to 60 °C in a thermostatted water bath behind a blast shield. A colour change from brown to orange was observed within 25 min. After this time, the tube was removed from the 60 °C bath, cooled in a room-temperature water bath (1 min), and then immediately inserted into the probe for ^{1}H NMR analysis.

^{1}H NMR (C_6D_6, 300 MHz; diagnostic signals; Figures S18, S20): δ 19.53 (q, $^3J_{HH}$ = 5.9 Hz, [Ru]=C*H*Me; none remaining), 9.62 (dt, $^3J_{HH}$ = 5.2 Hz, $^4J_{HH}$ = 1.5 Hz, 4H, py *o*-C*H* of **Ru-3**; 30%), 9.16 (br d, $^3J_{HH}$ = 4.2 Hz, 2H, py *o*-C*H* of **Ru-3'**; 48%), 8.00 (s, 4H, C*H* of DMT), 5.52–5.30 (overlapping m, 2H, =C*H* of *(E)*/*(Z)*-2-butene and 2-pentene, 53% total), 5.25 (s, 4H, C_2H_4, <1%), 5.06–4.90 (m, 2H, =CH_2 of propene, 23%). The overlapping olefinic signals for 2-butene and 2-pentene were deconvoluted by re-running the spectrum at 600 MHz (Figure S19). The observed proportion of butene, pentene, and propene increased on warming the sample to 60 °C in the probe, perhaps reflecting pressure buildup in the headspace on warming. ^{1}H NMR (C_6D_6, 300 MHz, 60 °C; diagnostic signals): δ 5.52–5.30 (m, 2H, =C*H* of *(E)*/*(Z)*-butene and 2-pentene, 69%), 5.06–4.88 (m, 2H, =CH_2 of propene, 24%). Adding 2 equiv pyridine to the reaction resulted in conversion of the Ru products to **Ru-3** (85%). The identities of the butene, pentene, and propene products were confirmed by ^{1}H and ^{13}C{^{1}H} NMR, ^{1}H–^{1}H COSY, ^{1}H–^{13}C HSQC, and ^{1}H–^{13}C HMBC analysis. The key NMR shifts are provided below.

(E)-2-butene: ^{1}H NMR (C_6D_6, 600 MHz): δ 5.38 (m, 2H, =C*H*), 1.57 (m, 6H, CH_3). ^{13}C{^{1}H} NMR (C_6D_6, 150 MHz): δ 124.5, 17.8. *(Z)-2-butene:* ^{1}H NMR (C_6D_6, 600 MHz): δ 5.48 (m, 2H, =C*H*), 1.51 (d, $^3J_{HH}$ = 5.0 Hz, 6H, CH_3). ^{13}C{^{1}H} NMR (C_6D_6, 150 MHz): δ 125.7, 12.0. The NMR signals are slightly shifted relative to the reported values in $CDCl_3$,[50] but are otherwise in good agreement.

Propene: ^{1}H NMR (C_6D_6, 600 MHz): δ 5.76–5.67 (m, 1H, =C*H*), 5.01 (dm, $^3J_{HH}$ = 17.0 Hz, =CH_2), 4.95 (dm, $^3J_{HH}$ = 10.3 Hz, =CH_2), 1.55 (dt, $^3J_{HH}$ = 6.5 Hz, $^4J_{HH}$ = 1.5 Hz). ^{13}C{^{1}H} NMR (C_6D_6, 150 MHz): δ 134.0 (=*C*H), 115.6 (=*C*H_2), 19.4 (*C*H_3). The observed shifts are in excellent agreement with the reported values.[49]

(E)-2-pentene: ^{1}H NMR (C_6D_6, 600 MHz): δ 5.52–5.33 (m, 2H, =C*H*), 1.94 (dq, $^3J_{HH}$ = 7.5 Hz, $^3J_{HH}$ = 1.3 Hz, 2H, =CHCH_2). ^{13}C{^{1}H} NMR (C_6D_6, 150 MHz): δ 133.0 (=*C*H), 122.8 (=*C*H), 26.0 (=CH*C*H_2). The NMR signals are slightly shifted relative to the reported values in $CDCl_3$, but are otherwise in good agreement.[51] A predominantly *(E)*-configuration is assigned on the basis of the downfield location of the =CHCH_2 singlet (δ_C 26.0, vs. 25.2 in $CDCl_3$; cf. 20.0 for *(Z)*-pentene in $CDCl_3$).[51]

Synthesis of $RuCl_2(H_2IMes)(o\text{-dianiline})(=CH_2)$, Ru-6. For the NMR-scale synthesis of **Ru-6**, see SI. In a 10 mL Schlenk flask, a 60 mM solution of **PII** (75 mg, 0.081 mmol) in CH_2Cl_2 (1.10 mL) was prepared and frozen in N_2(*l*). The headspace was evacuated, the flask was sealed, and the solution was allowed to thaw at –50 °C. Ethylene gas (1 atm) was then admitted via the side-arm, after which the flask was sealed again, and the reaction was stirred at –50 °C for 10 min, over which time the colour changed from dark brown to bright pink. A solution of *o*-dianiline (15.8 mg, 0.0855 mmol, 1.05 equiv) in CH_2Cl_2 (250 μL) was then added dropwise. Care was taken to dribble the solution down the cold wall of the flask, to avoid warming the reaction mixture. A colour change from pink to green occurred within 10 min. The solution was stirred for an additional 20 min, then cooled further to –78 °C (acetone–dry ice), after which cold pentane (30 mL; –78 °C) was added via cannula. To avoid warming, the cannula was kept cold with dry ice. The resulting precipitate was decanted and dried in vacuo to afford 74 mg of a pale green solid containing a near-equimolar mixture (1.2:1.0) of **Ru-6** and $[H_2C{=}CHPCy_3]OTf$,[10a] with ca. 10-15% unidentified Ru-H_2IMes impurities. Yield of crude **Ru-6**: 75%. Attempts at reprecipitation or washing caused decomposition into **Ru-7**. Given below are NMR details for **Ru-6** alone; those for the phosphonium salt appear in the supporting information.

^{1}H NMR ($CDCl_3$, 300 MHz, –50 °C; Figure S22): δ 19.46 (s, 2H, [Ru]=CH_2), 7.39 (s, 1H, Mes C*H*), 7.32–6.92 (m, 13H, Mes C*H* and *o*-dianiline C*H*; overlaps with residual C*H*Cl_3), 6.57 (br d, $^3J_{HH}$ = 7.8 Hz, 1H, *o*-dianiline C*H*), 6.44 (br d, $^3J_{HH}$ = 7.8 Hz, 1H, *o*-dianiline C*H*), 4.37 (br s, 2H, NH_2), 4.14–3.70 (m, 4H, NCH_2), 3.68 (br s, 1H, N$H_a$$H_b$), 3.41 (br s, 1H, N$H_a$$H_b$), 2.67 (s, 3H, C$H_3$), 2.50 (s, 3H, C$H_3$), 2.35 and 2.34 (overlapping s, 9H, CH_3), 2.23 (s, 3H, CH_3). Assignment of the NH_2 signals was confirmed by adding ca. 5 μL D_2O at –50 °C, and rapidly shaking the tube (1-2 sec) before re-immersing in the cold-bath.

^{13}C{^{1}H} NMR ($CDCl_3$, 77.5 MHz, –50 °C; Figure S23): δ 314.2 ([Ru]=*C*H_2, ^{1}H-detected by HMQC), 218.5 (*C*$_{NHC}$), 143.6, 139.8, 139.0, 138.9, 138.6, 138.4, 137.1, 134.8, 134.3, 131.1, 130.6, 130.4, 129.4, 129.2, 128.9, 128.4, 119.1, 115.8, 50.6 (N*C*H_2), 49.8 (N*C*H_2), 21.5 (*C*H_3), 21.4 (*C*H_3), 19.2 (*C*H_3), 19.0 (*C*H_3), 18.6 (*C*H_3), 18.5 (*C*H_3).

Synthesis of $RuCl_2(H_2IMes)(py)_n(=CH_2)$ (**GIIIm**: n = 2; **GIIIm'**: n = 1). The synthesis was undertaken using the method for **Ru-6** above, with several modifications to prevent decomposition and enable precipitation of the product: (i) use of lower temperatures (down to –116 °C); (ii) immediate workup after adding pyridine; and (iii) higher Ru concentrations (ca. 110 mM starting **PII**), to aid in precipitating the product. Use of stoichiometric pyridine was likewise essential, to prevent oiling out of the product.

In a 10 mL Schlenk flask, a 110 mM solution of **PII** (60 mg, 0.065 mmol) in CH_2Cl_2 (0.60 mL) was prepared and frozen in N_2(*l*). The headspace was evacuated, the flask was sealed, and the solution was allowed to thaw at –50 °C. Ethylene gas (1 atm) was then admitted via the side-arm, after which the flask was sealed again, and the reaction was stirred at –50 °C for 10 min. A colour change from dark brown to bright pink occurred over this time. The solution was cooled further, to –78 °C, and a solution of pyridine (10.3 μL, 0.132 mmol, 2.0 equiv) in pentane (150 μL) was added dropwise. A colour change

from pink to green occurred over the course of the addition. Cold pentane (8 mL; –116 °C; N_2(l)–ethanol bath) was then added via a cannula chilled with dry ice. The resulting precipitate was decanted and dried in vacuo to afford 59 mg of the mustard-yellow product accompanied by [H_2C=CHPCy_3]Cl, in a 2:3 ratio. Also present are unidentified Ru-H_2IMes impurities, which give rise to additional mesityl CH_3 peaks (Figure S27). Integration of the alkylidene singlets at –50 °C indicates a ca. 1:2 ratio of **GIIIm** and **GIIIm'**. Crude yield: ca. 60% based on **GIIIm/m'**. Attempts to purify by washing with cold pentane (–116 °C) afforded no improvement. ^{1}H NMR analysis was carried out at 0 °C in $CDCl_3$ (in which the complex is more stable than in CD_2Cl_2). Exchange averaging at this temperature results in a single alkylidene peak, greatly simplifying analysis. Sample decomposition occurs over 3–4 h, precluding ^{13}C{^{1}H} NMR analysis. ^{1}H NMR ($CDCl_3$, 300 MHz, 0 °C; Figure S27): δ 18.83 (s, 2H, [Ru]=CH_2), 8.67 (br s, 0.6H, py *o*-C*H*), 7.82 (br s, 2H, py *o*-C*H*), 7.51 (br s, 0.6H, py *m*-C*H*), 7.37 (br t, 0.3H, $^3J_{HH}$ = 7.0 Hz, py *p*-C*H*), 7.15 (br t, $^3J_{HH}$ = 7.0 Hz, 1H, py *p*-C*H*), 7.01 (s, 4H, Mes C*H* and py *m*-C*H*), 6.95 (s, 2H, Mes C*H*), 4.12 (m, 2H, NCH_2), 4.02 (m, 2H, NCH_2), 2.55 (s, 6H, CH_3), 2.35 (s, 6H, CH_3), 2.32 (s, 6H, CH_3). Exchange averaging of the bis- and mono-pyridine complexes results in a single set of signals at 0 °C (as also seen for **GIII** and its mono-pyridine derivative **GIII'**; see below). At –50 °C, pyridine exchange is retarded and two sets of signals emerge. ^{1}H NMR ($CDCl_3$, –50 °C; key signals only): δ 19.35 (br s, [Ru]=CH_2 for **GIIIm**, 30%), 18.63 (br s, [Ru]=CH_2 for **GIIIm'**, 70%). Adding pyridine (10 μL) to the NMR sample at –50 °C caused clean conversion to **GIIIm**. Key ^{13}C NMR signals (detected via ^{1}H–^{13}C HMQC in $CDCl_3$ at 0 °C): 305.1 (s, [Ru]=CH_2), 129.7 (s, Mes C*H*), 129.4 (s, Mes C*H*), 51.1 (s, NCH_2), 49.9 (s, NCH_2).

Bimolecular coupling of Ru-6: quantification of ethylene and formation of Ru-7. These experiments were carried out with the precautions against explosion described above. The sample was prepared in the glovebox, so that the septum-sealed, screw-capped NMR tube could be replaced with a J. Young NMR tube (see Figure S1; 2.15 mL capacity), and perturbation by oxygen could be more rigorously inhibited. While the lower operating temperature is then limited to –35 °C (the temperature of the glovebox freezer), this was deemed acceptable given rapid manipulation, as decomposition commences only at ca. –10 °C. In a representative experiment, crude **Ru-6** (ca. 30 mg, 0.022 mmol) and 1.7 mg DMT (40 μL of a 0.22 M stock solution in CD_2Cl_2) were added to a cold NMR tube bedded in a chilled (–35 °C) sand-bath. Cold CD_2Cl_2 (1.72 mL; used instead of C_7D_8 to improve the solubility of **Ru-6**) was added, and the solution was mixed using a chilled pipette. The tube was sealed, transferred to the instrument room in an ethylene glycol–dry ice bath (–20 °C), and inserted into an NMR probe pre-cooled to –20 °C, to measure the initial integration ratio of **Ru-6** vs. DMT. The sample was then ejected from the NMR probe, mixed briefly by shaking, and allowed to warm in a 23 °C water bath (blast shield; see above). Decomposition of **Ru-6** was monitored over 1 h at RT (^{1}H NMR). During this time the colour changed from green to brown. After 6 min: ^{1}H NMR (CD_2Cl_2, 300 MHz, RT; diagnostic signals only): δ 19.53 (s, 2H, [Ru]=CH_2 of **Ru-6**; 27%), 8.09 (s, 4H, C*H* of DMT), 5.40 (s, 4H, C_2H_4; 63%), 4.91 (d, $^2J_{HH}$ = 10.3 Hz, 1H, NH_2 of **Ru-7**; 55%). At 1 h: 2% **Ru-6**, 52% C_2H_4, 61% **Ru-7**. At 85 min: no **Ru-6** remaining, 53% C_2H_4, 55% **Ru-7**.

RuCl$_2$(H$_2$IMes)(*o*-dianiline) Ru-7. ^{1}H NMR (CD_2Cl_2, 300 MHz; Figure S25): δ 7.29–6.95 (m, 9H, Ar C*H* of *o*-dianiline and Mes C*H*), 6.94 (s, 2H, Mes C*H*), 6.86 (d, 1H, $^3J_{HH}$ = 7.7 Hz, Ar C*H* of *o*-dianiline), 6.18 (m, 1H, Ar C*H* of *o*-dianiline), 4.89 (d, $^2J_{HH}$ = 10.4 Hz, 1H, NH_aH_b), 4.20 (d, $^2J_{HH}$ = 10.4 Hz, 1H, NH_aH_b), 4.12–3.89 (m, 6H, NCH_2 and NH_aH_b), 2.56 (br s, 6H, Mes *o*-CH_3), 2.41 (s, 6H, Mes *o*-CH_3), 2.25 (s, 6H, Mes *p*-CH_3). The two N*H* doublets that overlap with the backbone NCH_2 protons of H_2IMes were located from their ^{1}H–^{1}H COSY correlations with the well-separated N*H* signals further downfield. The diastereotopic NH_aH_b pairs thus identified appear at: 4.89 / 3.95 ppm, and 4.20 / 4.04 ppm. ^{13}C{^{1}H} NMR (CH_2Cl_2, 77.5 MHz; Figure S26): δ 213.8 (C_{NHC}), 140.0, 139.7, 138.9 (br), 138.3 (br), 138.0, 130.7, 129.8 (br), 129.8 (Mes *C*H), 129.7, 129.4, 128.1, 127.9, 127.54, 127.45, 124.8, 124.2, 123.7, 122.9, 122.6, 122.3, 52.3 (NCH_2), 20.6 (Mes *p*-CH_3), 18.6 (br, Mes *o*-CH_3), 18.3 (Mes *o*-CH_3). MALDI-TOF MS (pyrene matrix), *m*/*z*: [**Ru-7**–H]$^+$ 661.141 (calc'd: 661.144).

Bimolecular coupling of GIIIm: quantification of ethylene (Figure S28). Experiment carried out as for **Ru-6** above, using solid **GIIIm/m'** (ca. 60 mg, 0.038 mmol) and TMB (0.47 mg) in CD_2Cl_2 (1.72 mL). After 20 min: δ 18.80 (s, 2H, [Ru]=CH_2 of **GIIIm**; none remaining), 8.99 (br d, $^2J_{HH}$ = 5.6 Hz, 2H, py *o*-C*H* of **Ru-3**, 12%), 8.60 (br s, 2H, py *o*-C*H* of **Ru-3'**, 4%), 6.07 (s, 3H, Ar C*H* of TMB), 5.40 (s, 4H, C_2H_4; 70%).

Kinetics studies. The rate of disappearance of the methylidene signal for **Ru-6** vs. DMT internal standard was measured as in the ethylene quantitation experiments above, but using a standard NMR-tube headspace, as quantification of evolved gases is irrelevant.

*Kinetics at High [Ru]$_0$ (ca. 20 mM **Ru-6**).* A J. Young tube was chilled in a sand-bath in the glovebox, loaded with solid **Ru-6** (17 mg, 0.012 mmol), cold CD_2Cl_2 (600 μL), and DMT (ca. 1 mg) in the glovebox, to give a Ru concentration of approximately 20 mM (based on **Ru-6** is 48% pure, based on ^{1}H NMR analysis indicating 1.15 equiv [H_2C=CHPCy_3]OTf and ca. 15% Ru-H_2IMes impurities in this particular sample). Decomposition of **Ru-6** was monitored over three half-lives. A linear depend-

ence on [**Ru-6**]$^{-1}$ (Figures 6 and S9) indicates that coupling is second-order at this concentration (k_{obs} = 0.12 ± 0.02 M^{-1} s^{-1}, based on two trials).

*Kinetics at Low [Ru]$_0$ (ca. 1 mM **Ru-6**).* As above, but with ca. 1 mg solid **Ru-6** and DMT (0.024 mg, 0.125 nmol; 5.0 μL of a 26 mM stock solution in CD_2Cl_2) in 600 μL CD_2Cl_2. A starting Ru concentration of ca. 1 mM was established via integration of the methylidene singlet vs. DMT at –20 °C. Decomposition of **Ru-6** was monitored at +10 °C to permit collection of sufficient scans for good signal-to-noise ratios. Analysis as above revealed a linear dependence on ln[**Ru-6**], indicating that bimolecular coupling is first-order in **Ru-6** at low concentrations (k_{obs} = (1.9 ± 0.3)*10^{-4} s^{-1}, based on two trials).

Rate Inhibition by Added o-Dianiline at Low [Ru]$_0$. Experiments with and without exogenous *o*-dianiline were conducted at RT, under conditions that otherwise correspond to the 1 mM experiments above. The proportion of **Ru-6** was assessed after 1 h. Control: 5% **Ru-6** remaining. With 4 equiv *o*-dianiline: 21% **Ru-6**.

Computational methods. *Geometry optimization*. All DFT calculations were performed with the Gaussian 09 suite of programs.[52] Geometry optimization were performed using Head-Gordon's long-range- and dispersion-corrected hybrid density functional ωB97XD[53-55] as implemented in Gaussian 09. This functional was chosen as it provides geometries in very good agreement with those of X-ray diffraction analysis of Ru metathesis catalysts and other homogeneous catalysts.[56] Ruthenium was described by the Stuttgart 28-electron relativistic effective core potential, termed ECP28MDF and retrieved from the Stuttgart/Cologne group website,[57,58] in combination with the accompanying correlation-consistent valence double-ζ plus polarization basis set (cc-pVDZ-PP)[57] retrieved from the EMSL basis set exchange database.[59] All remaining atoms were described by Dunning's correlation-consistent valence double-ζ plus polarization basis sets (cc-pVDZ),[60,61] as retrieved from the EMSL basis set exchange database.[59] Numerical integration was performed using the "ultrafine" grid of Gaussian 09. This grid specification defaults to the coarser "SG1" grid for analytical Hessian calculations using the CPHF procedure. The built-in Gaussian 09 stability check was carried out for all self-consistent field solutions prior to geometry optimization. Instable solutions were re-optimized to real, spin-restricted solutions. Geometries were then optimized using tight convergence criteria (max. force 1.5·10^{-5} a.u., RMS force 1.0·10^{-5} a.u., max. force 6.0·10^{-5} a.u., RMS force 4.0·10^{-5} a.u.), without symmetry constraints, and using default convergence criteria for the self-consistent field (SCF) optimization procedure (RMS change in density matrix < 1.0·10^{-8}, max. change in density matrix = 1.0·10^{-6}).

All stationary points were characterized by the eigenvalues of the analytically calculated Hessian matrix, confirming either a single imaginary frequency (for the transition state) or no imaginary frequencies (for minima). The only exception was **Ru-11**, for which the procedure described above returned an imaginary frequency *i*13cm^{-1}. This imaginary frequency was confirmed to be an artifact resulting from the above-mentioned default reduction of the grid quality in analytical frequency calculations in Gaussian 09.[62] Specifically requesting the "ultrafine" grid also in the CPHF-based frequency calculation confirmed all-positive curvature for this intermediate as well. The thermal correction for **Ru-11** was thus obtained from the latter vibrational analysis using the "ultrafine" integration grid, while the standard procedure described above was used for all species for which artifacts from the grid were not detected. The translational, rotational, and vibrational components of the thermal corrections to enthalpies and Gibbs free energies were calculated within the ideal-gas, rigid-rotor, and harmonic oscillator approximations, except that all frequencies below 100 cm^{-1} were shifted to 100 cm^{-1} when calculating the vibrational component of the entropy,[63,64] to prevent asymptotic behavior of the harmonic approximation for modes of very low frequencies (an approach termed the "quasi-harmonic approximation" in the following).

Intrinsic reaction coordinate (IRC)[65] calculations (using the local quadratic approximation algorithm (LQA)[66] connected intermediate **Ru-8** with transition state **Ru-9**.

Single-point energy calculations. All single-point energy calculations were performed with the Gaussian 09 implementation of the generalized gradient approximation functional of Perdew, Burke and Ernzerhof (PBE),[67] and included Grimme's D3 empirical dispersion term[68] with revised Becke-Johnson[69] damping parameters (together labeled PBE-D3M(BJ), for brevity).[70] Ruthenium was described by the ECP28MDF relativistic effective core potential,[57] accompanied by a correlation-consistent valence quadruple-ζ plus polarization basis set (ECP28MDF_VQZ),[57] both obtained from the Stuttgart/Cologne group website. Carbon and hydrogen atoms were described by valence quadruple-ζ plus polarization (EMSL: cc-pVQZ)[59] basis sets.[60] All other atoms were described by the valence quadruple-ζ plus polarization augmented with diffuse functions (EMSL: aug-cc-pVQZ),[59,60,71] Electrostatic and non-electrostatic solvation effects in dichloromethane were taken into account using the polarizable continuum model (PCM), in combination with the "Dis", "Rep", and "Cav" keywords and the built-in program values (dielectric constant, number density, etc.).[72] The solute cavity was constructed using the united atom topological model with atomic radii optimized for Hartree–Fock (termed "UAHF")[72d,73] Numerical integrations were performed with the "ultrafine" grid of Gaussian 09 and the self-consistent field (SCF) density-based convergence criterion was set to 10^{-5} (RMS

change in density matrix < $1.0\cdot10^{-5}$, max. change in density matrix = $1.0\cdot10^{-3}$).

Calculation of Gibbs free energies. Gibbs free energies were calculated at 298.15 K according to equation 1.

$$G^{CH_2Cl_2}_{PBE\text{-}D3M(BJ)} = E^{CH_2Cl_2}_{PBE\text{-}D3M(BJ)} + \Delta G^{T=298.15K}_{\varpi B97XD,qh} + \Delta G^{T=298.15K}_{1atm\rightarrow 1M} \quad (1)$$

Here $E^{CH_2Cl_2}_{PBE\text{-}D3M(BJ)}$ corresponds to the potential energies resulting from single point calculations with PBE-D3M(BJ), including the contributions from the implicit solvation model; $\Delta G^{T=298.15K}_{\varpi B97XD,qh}$ is the thermal correction to the Gibbs free energy, calculated at the geometry optimization level with the quasi-harmonic approximation, and $\Delta G^{T=298.15K}_{1atm\rightarrow 1M}$ is the standard-state correction corresponding to 1 M solution (but exhibiting infinite-dilution, ideal-gas-like behavior). The latter is equal to 1.89 kcal mol^{-1} (= RT·ln(24.46)). Table S5 reports all these values, together with the single-point energy calculated at the geometry optimization level ($E_{\varpi B97XD}$) and the corresponding Gibbs free energy including thermal corrections from the harmonic approximation ($G^{T=298.15K}_{\varpi B97XD}$).

Natural bond orbital analysis. The natural bond orbital analyses were performed using the NBO 6.0 program.[74] Memory restrictions prohibited NBO calculations on the dimeric ruthenium complexes (**Ru-8**, **Ru-13** and transition state **Ru-9**) using the very large basis sets for single-point calculations described above. Instead, Dunning's correlation-consistent valence triple-ζ plus polarization basis sets (cc-pVTZ-DK)[57,60,61] were used for all atoms in the single-point, self-consistent field calculations giving the electron density used in the NBO analyses. The remaining settings of the DFT model and the self-consistent field protocol were as described above for the single-point energy calculations, the sole exception being use of the original Becke-Johnson[69] damping parameters when calculating Grimme's D3 empirical dispersion terms.[68]

ASSOCIATED CONTENT

Supporting Information

Experimental procedures and NMR spectra, sample DFT input files, calculated energies, molecular structures and other properties (PDF). A file containing 3D rotatable images of all geometry-optimized structures as well as the IRC trajectory connecting transition state **Ru-9** with intermediate **Ru-8** (XYZ). This material is available free of charge via the Internet at http://pubs.acs.org.

AUTHOR INFORMATION

Corresponding Author

* Email: dfogg@uottawa.ca.

ACKNOWLEDGEMENT

This work was funded by NSERC of Canada and by the Research Council of Norway (RCN, project 262370). NSERC is thanked for fellowships to GAB and CSH, and RCN for a fellowship to MF, as well as CPU (NN2506K) and storage resources (NS2506K). Giovanni Occhipinti is thanked for useful discussions.

REFERENCES

(1) (a) Grela, K., *Olefin Metathesis-Theory and Practice*. Wiley: Hoboken, NJ, 2014. (b) Grubbs, R. H.; Wenzel, A. G., *Handbook of Metathesis*. 2nd ed.; Wiley-VCH: Weinheim, 2015.

(2) (a) Higman, C. S.; Lummiss, J. A. M.; Fogg, D. E. *Angew. Chem., Int. Ed.* **2016**, *55*, 3552–3565. (b) K. R. Fandrick, J. Savoie, N. Y. Jinhua, J. J. Song, C. H. Senanayake, In ref 1a, pp. 349-366. (c) Farina, V.; Horváth, A. In ref 1a, pp 633–658.

(3) Rate constants for initiation (k_i; x 10^{-3} s^{-1}) at 5 °C: **GII**, 0.0032; **HII**, 2.6; **GIII**, >200. See: Love, J. A.; Morgan, J. P.; Trnka, T. M.; Grubbs, R. H. *Angew. Chem., Int. Ed.* **2002**, *41*, 4035–4037, and references therein. % Recapture = proportion of the resting-state species at 50% catalyst decomposition during styrene metathesis (100 equiv styrene, 22 °C, C_6D_6). Data for selected Class A–C catalysts: **GII**, 15%; **HII**, 100%; **GIII**, 0%. The resting states are, respectively, $RuCl_2(H_2IMes)(PCy_3)(=CH_2)$ **GIIm**, **HII** itself, and (see below) $RuCl_2(H_2IMes)(py)_n(=CH_2)$.

(4) Higman, C. S.; Nascimento, D.; Ireland, B. J.; Audorsch, S.; Bailey, G. A.; Fogg, D. E. *J. Am. Chem. Soc.* **2018**, *140*, 1604−1607.

(5) For evidence of "boomerang" recapture of isopropoxystyrene, see: (a) Bates, J. M.; Lummiss, J. A. M.; Bailey, G. A.; Fogg, D. E. *ACS Catal.* **2014**, *4*, 2387−2394. (b) Griffiths, J. R.; Keister, J. B.; Diver, S. T. *J. Am. Chem. Soc.* **2016**, *138*, 5380−5391. For the original proposal, see: (c) Garber, S. B.; Kingsbury, J. S.; Gray, B. L.; Hoveyda, A. H. *J. Am. Chem. Soc.* **2000**, *122*, 8168–8179.

(6) The vinylphosphonium salt $[H_2C{=}CHPCy_3]Cl$ lost on initiation of **PII** does not re-enter metathesis. See: Leitao, E. M.; van der Eide, E. F.; Romero, P. E.; Piers, W. E.; McDonald, R. *J. Am. Chem. Soc.* **2010**, *132*, 2784–2794.

(7) (a) Schrodi, Y., Mechanisms of Olefin Metathesis Catalyst Decomposition and Methods of Catalyst Reactivation. In ref 1b, pp 323–342. (b) Chadwick, J. C.; Duchateau, R.; Freixa, Z.; van Leeuwen, P. W. N. M., Alkene Metathesis. In *Homogeneous Catalysts: Activity – Stability – Deactivation*, Wiley-VCH: Weinheim, 2011; pp 347-396.

(8) (a) Hong, S. H.; Wenzel, A. G.; Salguero, T. T.; Day, M. W.; Grubbs, R. H. *J. Am. Chem. Soc.* **2007**, *129*, 7961–7968. (b) Hong, S. H.; Day, M. W.; Grubbs, R. H. *J. Am. Chem. Soc.* **2004**, *126*, 7414–7415.

(9) (a) McClennan, W. L.; Rufh, S.; Lummiss, J. A. M.; Fogg, D. E. *J. Am. Chem. Soc.* **2016**, *138*, 14668−14677. (b) Lummiss, J. A. M.; McClennan, W. L.; McDonald, R.; Fogg, D. E. *Organometallics* **2014**, *33*, 6738–6741. (c) Lummiss, J. A. M.; Ireland, B. J.; Sommers, J. M.; Fogg, D. E. *ChemCatChem* **2014**, *6*, 459–463. (d) Lummiss, J. A. M.; Botti, A. G. G.; Fogg, D. E. *Catal. Sci. Technol.* **2014**, *4*, 4210–4218.

(10) (a) Romero, P. E.; Piers, W. E. *J. Am. Chem. Soc.* **2005**, *127*, 5032–5033. (b) Romero, P. E.; Piers, W. E. *J. Am. Chem. Soc.* **2007**, *129*, 1698–1704. (c) van der Eide, E. F.; Piers, W. E. *Nature Chem.* **2010**, *2*, 571–576.

(11) Solans-Monfort, X.; Coperet, C.; Eisenstein, O. *J. Am. Chem. Soc.* **2010**, *132*, 7750–7757.

(12) Nizovtsev, A. V.; Afanasiev, V. V.; Shutko, E. V.; Bespalova, N. B. *NATO Sci. Ser. II* **2007**, *243*, 125–135.

(13) Propene loss was also reported on reaction of **GII** with ethylene. See: van Rensburg, W. J.; Steynberg, P. J.; Meyer, W. H.; Kirk, M. M.; Forman, G. S. *J. Am. Chem. Soc.* **2004**, *126*, 14332–14333. Methylidene abstraction (refs 8,9) was apparently prevented by oxidation of PCy_3; $O{=}PCy_3$ was detected.

(14) Bailey, G. A.; Lummiss, J. A. M.; Foscato, M.; Occhipinti, G.; McDonald, R.; Jensen, V. R.; Fogg, D. E. *J. Am. Chem. Soc.* **2017**, *139*, 16446–16449.

(15) Ireland, B. J.; Dobigny, B. T.; Fogg, D. E. *ACS Catal.* **2015**, *5*, 4690–4698.

(16) Engel, J.; Smit, W.; Foscato, M.; Occhipinti, G.; Törnroos, K. W.; Jensen, V. R. *J. Am. Chem. Soc.* **2017**, *139*, 16609–16619.

(17) Williams, J. E.; Harner, M. J.; Sponsler, M. B. *Organometallics* **2005**, *24*, 2013–2015.

(18) Pyridine is significantly less nucleophilic than either PPh_3 or PCy_3. *N* values on the logarithmic Mayr nucleophilicity scale: pyridine, 12.90; PPh_3, 14.33; PCy_3, 14.64; all in dichloromethane. See: http://www.cup.lmu.de/oc/mayr/reaktionsdatenbank/.

(19) (a) Schrock, R. R.; Copéret, C. *Organometallics* **2017**, *36*, 1884–1892. An important early analysis noted the striking propensity of $M{=}CH_2$ species to eliminate ethylene: (b) Merrifield, J. H.; Lin, G.-Y.; Kiel, W. A.; Gladysz, J. A. *J. Am. Chem. Soc.* **1983**, *105*, 5811–5819. For crystallographically characterized examples of methylidene complexes derived from group 6 metathesis catalysts, see: (c) Arndt, S.; Schrock, R. R.; Muller, P. *Organometallics* **2007**, *26*, 1279–1290. (d) Tsang, W. C. P.; Jamieson, J. Y.; Aeilts, S. L.; Hultzsch, K. C.; Schrock, R. R.; Hoveyda, A. H. *Organometallics* **2004**, *23*, 1997–2007.

(20) (a) Fürstner, A.; Ackermann, L.; Gabor, B.; Goddard, R.; Lehmann, C. W.; Mynott, R.; Stelzer, F.; Thiel, O. R. *Chem. – Eur. J.* **2001**, *7*, 3236–3253. (b) Huang, J.; Schanz, H.-J.; Stevens, E. D.; Nolan, S. P. *Organometallics* **1999**, *18*, 5375–5380.

(21) Adlhart, C.; Chen, P. *Helv. Chim. Acta* **2003**, *86*, 941–949.

(22) Experiments in 2.00 mL total volume of C_6D_6 plus styrene, in a 2.15 mL J. Young tube. Further reductions in headspace present an explosion hazard (see SI).

(23) (a) Borguet, Y.; Sauvage, X.; Zaragoza, G.; Demonceau, A.; Delaude, L. *Organometallics* **2011**, *30*, 2730–2738 and references therein. (b) Wolf, J.; Thommes, K.; Briel, O.; Scopelliti, R.; Severin, K. *Organometallics* **2008**, *27*, 4464–4474. (c) Quebatte, L.; Solari, E.; Scopelliti, R.; Severin, K. *Organometallics* **2005**, *24*, 1404–1406.

(24) Reported pK_a values in acetonitrile. Pyridine: 12.6; NEt_3: 18.5. See: Cox, B. G., *Acids and Bases: Solvent Effects on Acid-Base Strength*. Oxford University Press: Croydon, 2013, p. 99–115.

(25) (a) Griffiths, J. R.; Hofman, E. J.; Keister, J. B.; Diver, S. T. *Organometallics* **2017**, *36*, 3043–3052. (b) Galan, B. R.; Pitak, M.; Gembicky, M.; Keister, J. B.; Diver, S. T. *J. Am. Chem. Soc.* **2009**, *131*, 6822–6832. (c) Galan, B. R.; Gembicky, M.; Dominiak, P. M.; Keister, J. B.; Diver, S. T. *J. Am. Chem. Soc.* **2005**, *127*, 15702–15703.

(26) For computational studies of Buchner insertion of methylidene: (a) Poater, A.; Ragone, F.; Correa, A.; Cavallo, L. *J. Am. Chem. Soc.* **2009**, *131*, 9000-9006. Of benzylidene: (b) Poater, A.; Cavallo, L. *Theor. Chem. Acc.* **2012**, *131*, 1155.

(27) Primary evidence is the unperturbed H_2IMes ligand in **Ru-3** (quantitative). In addition, reaction of **GIIIm/m′** with cyclohexene revealed no norcarane resulting from cyclopropanation by ^{1}H NMR or GC-MS analysis. Instead, ethylene is generated, consistent with decomposition by bimolecular coupling. A further possibility suggested by a referee, involving loss of alkylidene as the free carbene on binding a π-acceptor ligand, was explicitly ruled out in the Cavallo study (ref 26a) on the basis of the high energy barriers involved. Diver's studies likewise suggested that alkylidene insertion is intramolecular (see ref 25b).

(28) Sanford, M. S.; Love, J. A.; Grubbs, R. H. *Organometallics* **2001**, *20*, 5314–5318.

(29) Walsh, D. J.; Lau, S. H.; Hyatt, M. G.; Guironnet, D. *J. Am. Chem. Soc.* **2017**, *139*, 13644–13647.

(30) Adding pyridine to the solution, with the intention of converting all Ru species present to **Ru-3**, left a shortfall of ca. 25%. Ru nanoparticles may account for the balance of material: see (a) Higman, C. S.; Lanterna, A. E.; Marin, M. L.; Scaiano, J. C.; Fogg, D. E. *ChemCatChem* **2016**, *8*, 2446–2449. The chief alternative possibility, formation of paramagnetic Ru byproducts, is improbable given the absence of significant signal broadening in the NMR spectrum (Figure S14).

(31) Lummiss, J. A. M.; Beach, N. J.; Smith, J. C.; Fogg, D. E. *Catal. Sci. Technol.* **2012**, *2*, 1630–1632.

(32) (a) Schwab, P.; Grubbs, R. H.; Ziller, J. W. *J. Am. Chem. Soc.* **1996**, *118*, 100–110. (b) Werner, H.; Stuer, W.; Weberndorfer, B.; Wolf, J. *Eur. J. Inorg. Chem.* **1999**, 1707–1713. (c) Burrell, A. K.; Clark, G. R.; Rickard, C. E. F.; Roper, W. R.; Wright, A. H. *J. Chem. Soc., Dalton Trans.* **1991**, 609–614.

(33) PCy_3 loss from **GIIm** is >40,000x slower than from **GI**, $RuCl_2(PCy_3)_2(=CHPh)$. See: (a) Lummiss, J. A.; Higman, C. S.; Fyson, D. L.; McDonald, R.; Fogg, D. E. *Chem. Sci.* **2015**, *6*, 6739–6746. (b) Lummiss, J. A.; Perras, F. A.; Bryce, D. L.; Fogg, D. E. *Organometallics* **2016**, *35*, 691–698.

(34) The excellent Lewis basicity of *o*-dianiline is evident from over a dozen reports of its Ru complexes. Selected examples: (a) Crimmin, M. R.; Bergman, R. G.; Toste, F. D. *Angew. Chem., Int. Ed.* **2011**, *50*, 4484–4487. (b) Faller, J. W.; Fontaine, P. P. *Organometallics* **2005**, *24*, 4132–4138. (c) Aikawa, K.; Mikami, K. *Angew. Chem., Int. Ed.* **2003**, *42*, 5455–5458. A pK_a of 3.81 in 70% aqueous EtOH is reported for the conjugate acid of *o*-dianiline; cf. 3.66 for pyridine. See, respectively: (a) Grantham, P. H.; Weisburger, E. K.; Weisburger, J. H. *J. Org. Chem.* **1961**, *26*, 1008–1017. (b) McDaniel, D. H.; Özcan, M. *J. Org. Chem.* **1968**, *33*, 1922–1923. The pK_a reported for pyridine in acetonitrile is considerably higher: see ref 24.

(35) Nickel, A.; Ung, T.; Mkrtumyan, G.; Uy, J.; Lee, C. W.; Stoianova, D.; Papazian, J.; Wei, W.-H.; Mallari, A.; Schrodi, Y.; Pederson, R. L. *Top. Catal.* **2012**, *55*, 518–523.

(36) Schweitzer, D.; Snell, K. D. *Org. Process Res. Dev.* **2015**, *19*, 715–720.

(37) Vignon, P.; Vancompernolle, T.; Couturier, J.-L.; Dubois, J.-L.; Mortreux, A.; Gauvin, R. M. *ChemSusChem* **2015**, *8*, 1143–1146.

(38) For PCy_3-stabilized catalysts, the greater steric bulk of the ethylidene ligand, vs. methylidene, also retards abstraction of this ligand by phosphine. See ref 9a.

(39) MacNaughtan, M. L.; Gary, J. B.; Gerlach, D. L.; Johnson, M. J. A.; Kampf, J. W. *Organometallics* **2009**, *28*, 2880–2887.

(40) Leitao, E. M.; Dubberley, S. R.; Piers, W. E.; Wu, Q.; McDonald, R. *Chem. – Eur. J.* **2008**, *14*, 11565–11572.

(41) For selected examples of transoid diruthenium complexes arising from decomposition of Ru-H2IMes catalysts, see refs 39, 40.

(42) Foster, J. P.; Weinhold, F. *J. Am. Chem. Soc.* **1980**, *102*, 7211–7218.

(43) Wiberg, K. B. *Tetrahedron* **1968**, *24*, 1083–1096.

(44) Occhipinti, G.; Jensen, V. R. *Organometallics* **2011**, *30*, 3522–3529.

(45) Jung, K.-H.; Kim, H.-K.; Lee, G. H.; Kang, D.-S.; Park, J.-A.; Kim, K. M.; Chang, Y.; Kim, T.-J. *J. Med. Chem.* **2011**, *54*, 5385–5394.

(46) Bottomley, F.; Mukaida, M. *J. Chem. Soc., Dalton Trans.* **1982**, 1933–1937.

(47) van Lierop, B. J.; Reckling, A. M.; Lummiss, J. A. M.; Fogg, D. E. *ChemCatChem* **2012**, *4*, 2020–2025.

(48) Dubberley, S. R.; Romero, P. E.; Piers, W. E.; McDonald, R.; Parvez, M. *Inorg. Chim. Acta* **2006**, *359*, 2658–2664.

(49) Fulmer, G. R.; Miller, A. J. M.; Sherden, N. H.; Gottlieb, H. E.; Nudelman, A.; Stoltz, B. M.; Bercaw, J. E.; Goldberg, K. I. *Organometallics* **2010**, *29*, 2176–2179.

(50) Wang, R.; Groux, L. F.; Zargarian, D. *Organometallics* **2002**, *21*, 5531–5539.

(51) Lucke, A. J.; Young, D. J. *J. Org. Chem.* **2005**, *70*, 3579–3583.

(52) Frisch, M. J.; Trucks, G. W.; Schlegel, H. B.; Scuseria, G. E.; Robb, M. A.; Cheeseman, J. R.; Scalmani, G.; Barone, V.; Mennucci, B.; Petersson, G. A.; Nakatsuji, H.; Caricato, M.; Li, X.; Hratchian, H. P.; Izmaylov, A. F.; Bloino, J.; Zheng, G.; Sonnenberg, J. L.; Hada, M.; Ehara, M.; Toyota, K.; Fukuda, R.; Hasegawa, J.; Ishida, M.; Nakajima, T.; Honda, Y.; Kitao, O.; Nakai, H.; Vreven, T.; Montgomery, J. A.; Peralta, J. E.; Ogliaro, F.; Bearpark, M.; Heyd, J. J.; Brothers, E.; Kudin, K. N.; Staroverov, V. N.; Keith, T.; Kobayashi, R.; Normand, J.; Raghavachari, K.; Rendell, A.; Burant, J. C.; Iyengar, S. S.; Tomasi, J.; Cossi, M.; Rega, N.; Millam, J. M.; Klene, M.; Knox, J. E.; Cross, J. B.; Bakken, V.; Adamo, C.; Jaramillo, J.; Gomperts, R.; Stratmann, R. E.; Yazyev, O.; Austin, A. J.; Cammi, R.; Pomelli, C.; Ochterski, J. W.; Martin, R. L.; Morokuma, K.; Zakrzewski, V. G.; Voth, G. A.; Salvador, P.; Dannenberg, J. J.; Dapprich, S.; Daniels, A. D.; Farkas, O.; Foresman, J. B.; Ortiz, J. V.; Cioslowski, J.; Fox, D. J., Gaussian 09, Revision D.01, Gaussian, Inc., Wallingford CT. 2013.

(53) Becke, A. D. *J. Chem. Phys.* **1997**, *107*, 8554–8560.

(54) Wu, Q.; Yang, W. *J. Chem. Phys.* **2002**, *116*, 515–524.

(55) Chai, J.-D.; Head-Gordon, M. *Phys. Chem. Chem. Phys.* **2008**, *10*, 6615–6620.

(56) Minenkov, Y.; Singstad, Å.; Occhipinti, G.; Jensen, V. R. *Dalton Trans.* **2012**, *41*, 5526–5541.

(57) Peterson, K. A.; Figgen, D.; Dolg, M.; Stoll, H. *J. Chem. Phys.* **2007**, *126*, 124101.

(58) Energy-consistent pseudopotentials of the Stuttgart/Cologne Group, http://www.tc.uni-koeln.de/PP/clickpse.en.html.

(59) (a) Feller, D. *J. Comput. Chem.* **1996**, *17*, 1571–1586. (b) Schuchardt, K. L.; Didier, B. T.; Elsethagen, T.; Sun, L.; Gurumoorthi, V.; Chase, J.; Li, J.; Windus, T. L. J. *Chem. Inf. Model.* **2007**, *47*, 1045–1052.

(60) Dunning, T. H. *J. Chem. Phys.* **1989**, *90*, 1007–1023.

(61) Woon, D. E.; Dunning, T. H. *J. Chem. Phys.* **1993**, *98*, 1358–1371.

(62) Martin, J. M. L.; Bauschlicher, C. W.; Ricca, A. *Comput. Phys. Commun.* **2001**, *133*, 189–201.

(63) Zhao, Y.; Truhlar, D. G. *Phys. Chem. Chem. Phys.* **2008**, *10*, 2813–2818.

(64) Ribeiro, R. F.; Marenich, A. V.; Cramer, C. J.; Truhlar, D. G. *J. Phys. Chem. B* **2011**, *115*, 14556–14562.

(65) Fukui, K. *Acc. Chem. Res.* **1981**, *14*, 363–368.

(66) (a) Page, M.; Doubleday, C.; McIver, J. W. *J. Chem. Phys.* **1990**, *93*, 5634–5642. (b) Page, M.; McIver, J. W. *J. Chem. Phys.* **1988**, *88*, 922–935.

(67) (a) Perdew, J. P.; Burke, K.; Ernzerhof, M. *Phys. Rev. Lett.* **1996**, *77*, 3865–3868. (b) Perdew, J.; Burke, K.; Ernzerhof, M. *Phys. Rev. Lett*. **1997**, *78*, 1396–1396.

(68) Grimme, S.; Ehrlich, S.; Goerigk, L. *J. Comput. Chem.* **2011**, *32*, 1456–1465.

(69) Johnson, E. R.; Becke, A. D. *J. Chem. Phys.* **2005**, *123*, 024101.

(70) Smith, D. G. A.; Burns, L. A.; Patkowski, K.; Sherrill, C. D. *J. Phys. Chem. Lett.* **2016**, *7*, 2197–2203.

(71) Kendall, R. A.; Dunning, T. H.; Harrison, R. J. *J. Chem. Phys.* **1992**, *96*, 6796–6806.

(72) (a) Cossi, M.; Scalmani, G.; Rega, N.; Barone, V. *J. Chem. Phys.* **2002**, *117*, 43–54. (b) Scalmani, G.; Frisch, M. J. *J. Chem. Phys.* **2010**, *132*, 114110. (c) Tomasi, J.; Mennucci, B.; Cammi, R. *Chem. Rev.* **2005**, *105*, 2999–3093. (d) Tomasi, J.; Persico, M. *Chem. Rev.* **1994**, *94*, 2027–2094.

(73) (a) Tomasi, J. *Theor. Chem. Acc.* **2004**, *112*, 184–203. (b) Cramer, C. J.; Truhlar, D. G. *Phys. Chem. Chem. Phys.* **2009**, *11*, 10757–10816. (c) Klamt, A.; Mennucci, B.; Tomasi, J.; Barone, V.; Curutchet, C.; Orozco, M.; Luque, F. J. *Acc. Chem. Res.* **2009**, *42*, 489–492.

(74) Glendening, E. D.; Badenhoop, J. K.; Reed, A. E.; Carpenter, J. E.; Bohmann, J. A.; Morales, C. M.; Landis, C. R.; Weinhold, F. *NBO*, 6.0.; Theoretical Chemistry Institute, University of Wisconsin: Madison, WI, 2013.

TOC graphic

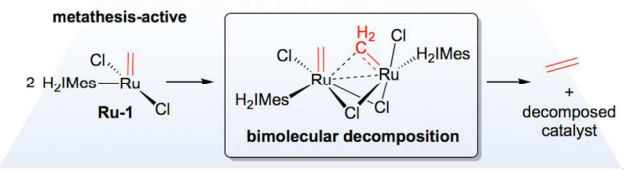
metathesis-active
2 H2IMes—Ru
Cl
Cl
Ru-1
H2
C
Cl
Cl
H2IMes
Ru
Ru
H2IMes
Cl
Cl
bimolecular decomposition
+
decomposed
catalyst